Short-Term Synaptic Dynamics Control the Activity Phase of Neurons in an Oscillatory Network

Abbreviated Title: Synaptic dynamics influence activity phase of oscillatory neurons

Authors: Diana Martinez[1*], Haroon Anwar[1], Amitabha Bose[2], Dirk Bucher[1], Farzan Nadim[1,2]

1 Federated Department of Biological Sciences, New Jersey Institute of Technology and Rutgers University, Newark, NJ 07102.

2 Department of Mathematical Sciences, New Jersey Institute of Technology, Newark, NJ 07102.

* Current Address: Department of Biomedical Sciences and Dalton Cardiovascular Research Center, University of Missouri, 134 Research Park Dr., Columbia, MO 65211, USA

Corresponding Author: Farzan Nadim, New Jersey Institute of Technology, Department of Biological Sciences, 323 Martin Luther King Blvd, Newark, NJ 07102, Phone (973) 596-8453, Email: farzan@njit.edu

Abstract

In oscillatory systems, neuronal activity phase is often independent of network frequency. Such phase maintenance requires adjustment of synaptic input with network frequency, a relationship that we explored using the crab, *Cancer borealis*, pyloric network. The burst phase of pyloric neurons is relatively constant despite a >2-fold variation in network frequency. We used noise input to characterize how input shape influences burst delay of a pyloric neuron, and then used dynamic clamp to examine how burst phase depends on the period, amplitude, duration, and shape of rhythmic synaptic input. Phase constancy across a range of periods required a proportional increase of synaptic duration with period. However, phase maintenance was also promoted by an increase of amplitude and peak phase of synaptic input with period. Mathematical analysis shows how short-term synaptic plasticity can coordinately change amplitude and peak phase to maximize the range of periods over which phase constancy is achieved.

150/150

Introduction

Oscillatory neural activity is often organized into different phases across groups of neurons, both in brain rhythms associated with cognitive tasks or behavioral states (Hasselmo et al., 2002; Buzsaki and Wang, 2012; Buzsaki and Tingley, 2018), and in central pattern generating (CPG) circuits that drive rhythmic motor behaviors (Marder and Bucher, 2001; Marder et al., 2005; Grillner, 2006; Bucher et al., 2015; Katz, 2016; Stein, 2018). The functional significance of different phases in the latter is readily apparent, as they for example provide alternating flexion and extension of limb joints, and coordination of movements between joints, limbs, and segments (Krantz and Parks, 2012; Grillner and El Manira, 2015; Kiehn, 2016; Le Gal et al., 2017; Bidaye et al., 2018). A hallmark of many such patterns is that the relative timing of firing between neurons is well maintained over a range of rhythm frequencies (Dicaprio et al., 1997; Hooper, 1997b, a; Wenning et al., 2004; Marder et al., 2005; Grillner, 2006; Mullins et al., 2011; Le Gal et al., 2017). If the latency of firing across different groups of neurons changes proportionally to the rhythm period, phase (latency over period) is invariant, in some cases providing optimal limb coordination at all speeds (Zhang et al., 2014).

The ability of the system to coordinate phases with changes in period arises from central coordinating mechanisms between circuit elements, as it is present in isolated nervous system preparations, but the underlying cellular and circuit mechanisms are not well understood. For instance, constant phase lags between neighboring segments in the control of swimming in lamprey fish and crayfish can be explained mathematically on the basis of asymmetrically weakly coupled oscillators, but the role of intrinsic and synaptic dynamics within each segment is unknown (Cohen et al., 1992; Skinner and Mulloney, 1998; Grillner, 2006; Mullins et al., 2011; Zhang et al., 2014; Le Gal et al., 2017).

The pyloric circuit of the crustacean stomatogastric ganglion (STG) has inspired a series of experimental and theoretical studies of cellular and synaptic mechanisms underlying phase maintenance. The pyloric circuit generates a triphasic motor pattern with stable phase relationships over a wide range of periods (Eisen and Marder, 1984; Hooper, 1997b, a; Bucher et al., 2005; Goaillard et al., 2009; Tang et al., 2012; Soofi et al., 2014). Synapses in the pyloric circuit use graded as well as spike-mediated transmission (Graubard et al., 1980; Harris-Warrick and Johnson, 2010; Zhao et al., 2011; Rosenbaum and Marder, 2018). Follower neurons burst in rebound from inhibition from pacemaker neurons (Marder and Bucher, 2007; Daur et al., 2016), and post-inhibitory rebound delay scales with the period of hyperpolarizing currents (Hooper, 1998). Voltage-gated conductances slow enough for cumulative activation across cycles could promote such phase maintenance (Hooper et al., 2009). Similarly, short-term depression of graded inhibitory synapses is slow enough to accumulate over several pyloric cycles, meaning that effective synaptic strength increases with increasing cycle period (Manor et al., 1997; Nadim and Manor, 2000).

Theoretical studies have shown that short-term synaptic depression, by increasing inhibition strength with cycle period, should promote phase maintenance (Manor et al., 2003; Mouser et al., 2008), particularly in conjunction with inactivating (A-type) potassium currents (Bose et al., 2004; Greenberg and Manor, 2005), which control the rebound delay (Harris-Warrick et al., 1995b; Harris-Warrick et al., 1995a; Kloppenburg et al., 1999). These predictions remain experimentally untested.

Additionally, postsynaptic responses also depend on the actual trajectory of synaptic conductances, which are shaped by presynaptic voltage trajectories and short-term synaptic plasticity (Manor et al., 1997; Mamiya et al., 2003; Zhao et al.,

2011; Tseng et al., 2014). If amplitude, duration, and trajectory of synaptic conductance determine rebound delay, phase maintenance necessitates all three of these parameters to change with cycle period in coordination. We used the dynamic clamp technique to exhaustively explore the range of these parameters and understand how the coordinated changes in synaptic dynamics determines the phase of follower neurons in an oscillatory circuit. Our findings are consistent with a mathematical framework that accounts for the dependence of amplitude and peak phase of the synaptic conductance on cycle period.

Results

Phase maintenance and latency maintenance

The firing of neurons in oscillatory networks is shaped by a periodic synaptic input. The relative firing latency of such neurons is often measured relative to a defined reference time in each cycle of oscillation, and is used to determine the activity phase of the neuron (see, e.g., Belluscio et al., 2012). For example, in a simple network consisting of a bursting oscillatory neuron driving a follower neuron (Fig. 1A1), at a descriptive level, the latency (Δt) of the follower neuron activity relative to the onset of the oscillator's burst onset may depend on the oscillation cycle period (P). In response to a change in period (say, to P_2), the follower neuron may keep constant latency ($\Delta t_2 = \Delta t$), or constant phase, i.e., modify its latency proportionally to the change in period ($\Delta t_2 / P_2 = \Delta t / P$; Fig. 1A2). However, in many oscillatory systems, for example the pyloric circuit (Hooper, 1997b, a), the relationship between L and P falls between these two extremes.

We demonstrated this point in the pyloric follower LP neuron using the following protocol. We voltage clamped one of the pacemaker PD neurons and drove this neuron with its own pre-recorded waveform, but applied at five different cycle periods (P). This protocol entrained the pacemaker group at this period, which forced the follower LP neuron to obey the same period (Fig. 1B). We then measured the latency (Δt) of the LP burst onset with respect to onset of the PD neuron burst. A plot of the LP latency Δt or phase ($\Delta t / P$) for different cycle periods demonstrates the above-mentioned finding that the LP neuron activity falls between the two limits of constant phase and constant latency (Fig. 1C).

The burst onset time of the LP neuron depends on the temporal dynamics of its input

The LP neuron does not have intrinsic oscillatory properties, but oscillates due to the synaptic input it receives from the pacemaker anterior burster (AB) and pyloric dilator (PD) neurons, and the follower pyloric constrictor (PY) neurons (Fig. 2A). The burst onset phase of the LP neuron ($\varphi_{LP} = \Delta t / P$; Fig. 2A) is shaped by the interaction between synaptic inputs and the neuron's intrinsic dynamics that influence post-inhibitory rebound. We measured an overall burst onset phase of the LP neuron of φ_{LP} =0.34 ± 0.03 (N=9).

As a first-order quantification, we measured how inputs to the LP neuron interact with its intrinsic properties to determine the timing between its bursts, in the absence of network oscillations. To this end, we blocked the synaptic input from the pacemaker AB and follower PY neurons to the LP neuron (Fig. 2B) and drove the LP neuron with a noise current input (see Methods). In response to the noise input, the LP neuron produced an irregular pattern of spike times, which included a variety of bursting patterns with different spike numbers (Fig. 2C). We were interested in the characteristics of inputs producing different burst onset latencies. However, unlike a periodic input, noise input does not provide a well-defined reference point to measure the burst onset latency. We categorized bursts with respect to the preceding inter-burst intervals (IBIs; see Methods), during which no other action potentials occurred. We classified these IBIs in bins (300, 500, 700 and 900 ms) and tagged bursts based on the IBI values (Fig. 2C). We characterized the driving input leading to bursts with specific IBIs by burst-triggered averaging the input current (I_{BTA}; an example shown in Fig. 2D). Our analysis produced a single I_{BTA} for each of the four IBIs in each preparation (N=23). I_{BTA}'s of each preparation were first normalized in amplitude by the (negative) peak value of the I_{BTA} at IBI = 300 ms (Fig. 2E; average shown in Fig. 2F) to examine how peak amplitude (I_{peak}) varied with IBI. These data were then normalized in time (Fig. 2G) to examine the effect of IBI on peak phase (Δ_{peak}) and the rise ($slope_{up}$) and fall ($slope_{down}$) slopes of the input current across preparations. We found that IBI had a significant effect on I_{peak}, Δ_{peak}, $slope_{up}$ and $slope_{down}$ (all one-way RM-ANOVA on ranks; data included in Figure 2-source data). In particular, larger IBIs corresponded to larger I_{peak} values (Fig. 2F-2H; $p<0.001$, $\chi^2 = 65.87$) with smaller (more advanced) Δ_{peak} (Fig. 2I; $p<0.001$, $\chi^2 = 41.35$). The change in Δ_{peak} was due to a decrease in

147 $slope_{up}$ ($p<0.001$, $\chi^2 = 65.25$), whereas $slope_{down}$ did not vary as much (Figs. 2J-2K;
148 $p=0.002$, $\chi^2 = 14.77$).

149 *The burst onset phase of the LP neuron oscillation depends on its synaptic input*

150 Injection of noise current revealed that the timing of the LP response is
151 exquisitely sensitive to the duration and amplitude of inputs. In the intact system, the
152 primary determinant of input duration and amplitude is the network period (*P*), as
153 increasing *P* increases both presynaptic pacemaker burst duration (Hooper, 1997b, a)
154 and synaptic strength (Manor et al., 1997; Nadim and Manor, 2000). To explore the
155 effect of the duration and strength of the synaptic input, we used dynamic clamp to
156 drive the LP neuron with a realistic synaptic conductance waveform.

157 We constructed this realistic waveform by measuring the synaptic current input
158 to the LP neuron during ongoing pyloric oscillations (Fig. 3A). These measurements
159 showed the two components of inhibitory synaptic input: those from the pacemaker AB
160 and PD neurons (left arrow) and those from the follower PY neurons (right arrow). In
161 each cycle, the synaptic current always had a single peak, but the amplitude and
162 phase of this peak showed variability across preparations (Fig. 3B, average in blue).

163 The realistic conductance input was injected periodically with strength g_{max} (Fig.
164 3C). For any fixed g_{max}, φ_{LP} decreased as a function of *P* (Fig. 3D), i.e., the relative
165 onset of the LP burst was advanced in slower rhythms. In contrast to the effect of *P*, for
166 any given *P*, φ_{LP} increased sublinearly as a function of g_{max} (Fig. 3E). Fig. 3F combines
167 the simultaneous influence of both parameters on φ_{LP}. The results shown in Fig. 3D
168 indicate that the LP neuron intrinsic properties alone do not produce phase constancy.
169 However, level sets of φ_{LP} (highlighted for three values in Fig. 3F), indicate that phase
170 could be maintained over a range of *P* values, if g_{max} increases as a function of *P.* This
171 finding was predicted by our previous modeling work, in which we suggested that
172 short-term synaptic depression promotes phase constancy by increasing synaptic
173 strength as a function of *P* (Manor et al., 2003; Bose et al., 2004). We will further
174 discuss the role of synaptic depression below.

175 To clarify the results of Fig. 3, it is worth examining the extent of phase
176 maintenance for fixed g_{max}. An example of this is shown in Fig. 4A (turquoise plots). A
177 comparison of these data with the theoretical cases in which either delay or phase is
178 constant suggests that the LP neuron produces relatively good phase maintenance, at

179 least much better in comparison with constant delay. However, this conclusion is
180 misleading because, in these experiments, the duty cycle of the synaptic input was
181 kept constant. Therefore, most of the phase maintenance is due the fact that the
182 synaptic input keeps perfect phase. In fact, if the reference point measures phase
183 relative to the end –rather than onset– of the PD burst (Fig. 4B), phase maintenance of
184 the LP neuron is barely better than in the constant delay case (Fig. 4A, purple plots). It
185 is therefore clear that phase maintenance by the LP neuron would require the
186 properties of the synaptic input to change as a function of P, a hallmark of short-term
187 synaptic plasticity (Fortune and Rose, 2001; Grande and Spain, 2005). As mentioned
188 above, short-term plasticity such as depression could produce changes in g_{max} as a
189 function of P. Independently of g_{max}, the peak time of the synaptic current is another
190 parameter that could change with P and influence the timing of the postsynaptic burst.
191 We therefore proceeded to systematically explore the influence of P, g_{max} and the
192 synaptic peak time on φ_{LP}.

193 *A systematic exploration of synaptic input parameters on the phase of the LP neuron*

194 For a detailed exploration of the influence of the synaptic input on φ_{LP}, we
195 approximated the trajectory of the (unitary) synaptic conductance in one cycle by a
196 simple triangle (Fig. 5A), which could be defined by three parameters: duration (T_{act}),
197 peak time (t_{peak}) and amplitude (g_{max}) (Fig. 5B). This simplified triangular synaptic
198 conductance waveform could then be repeated with any period (P) to mimic the
199 realistic synaptic input to the LP neuron. For a given synaptic duration T_{act}, the peak
200 phase of the synapse can be defined as $\Delta_{peak} = t_{peak} / T_{act}$). The parameter Δ_{peak} is
201 known to vary as a function of P (Tseng et al., 2014) and, in a previous study, we found
202 that Δ_{peak} may influence the activity of the postsynaptic neuron, independent of P and
203 g_{max} (Mamiya and Nadim, 2004). We therefore systematically explored the influence of
204 three parameters of the synaptic input (P, g_{max} and Δ_{peak}) on φ_{LP}.

205 As with the realistic synaptic waveforms (Fig. 3), we used the dynamic clamp
206 technique to apply the triangular conductance waveform periodically to the LP neuron
207 in the presence of the synaptic blocker picrotoxin. Across different runs within the same
208 experiment, the parameters P, g_{max} and Δ_{peak} were changed on a grid (see Methods). In
209 addition, all combinations of these three parameter values were run in two conditions in
210 the same experiment, 1: with constant duration, i.e., constant T_{act} across different P
211 values (C-Dur of 300 ms), and 2: with constant duty cycle, i.e., T_{act} changing

proportionally to P (C-DC of 0.3; Fig. 5C). Using these protocols, we measured the effects of synaptic parameters on φ_{LP} (Fig. 5D).

The LP neuron produced burst responses that followed the synaptic input in a 1:1 manner across all values of P that were used (Fig. 6A1). When g_{max} and Δ_{peak} were kept constant, φ_{LP} decreased as a function of P (Fig. 6A2). This decrease was always larger for the C-Dur case than the C-DC case. For both C-DC and C-Dur, this trend was seen across all values of Δ_{peak} and g_{max} (Fig 6A3). The effect of P on φ_{LP} was highly significant for both C-DC (Three-Way ANOVA, $p<0.001$, $F=100.677$) and C-Dur (Three-Way ANOVA, $p<0.001$, $F=466.424$), indicating that the period and duration of the inhibitory input to the LP neuron had a significant effect on its phase.

Changing g_{max} produced a large effect on the level of hyperpolarization in the LP neuron, but this usually translated to only a small or modest effect on the time to the first spike following inhibition (Fig. 6B1). Overall, increasing g_{max} at constant values of P and Δ_{peak} produced a significant but only small to moderate increase in φ_{LP} (Three-Way ANOVA, $p<0.001$, $F=10.798$). Although increasing g_{max} produced the same qualitative effect for both the C-DC and C-Dur (e.g., Fig. 6B2), φ_{LP} in the C-DC case was restricted to a smaller range (Fig. 6B3 top vs. bottom panels). Overall, this increase was robust for most values of P and Δ_{peak} (Fig. 6B3).

Increasing Δ_{peak} for a constant value of P and g_{max} (Fig. 6C1), produced a small but significant increase in φ_{LP} (Three-Way ANOVA, $p<0.001$, $F=17.172$). This effect was robust for most values of P and g_{max}, for both C-DC and C-Dur (Fig. 6C2 and 6C3).

These results showed that all three parameters that define the shape of the IPSC influence φ_{LP}. Clearly, the strongest effect is the decrease in φ_{LP} as a function of P. However, φ_{LP} modestly increases as a function of the other two parameters, g_{max} and Δ_{peak}. This raised the question how g_{max} and Δ_{peak} would have to change in coordination as a function of P to counteract the effect of P on φ_{LP} and achieve phase constancy.

Coordinated changes of g_{max} and Δ_{peak} produce the largest effect on phase

To explore how g_{max} and Δ_{peak} might interact to influence φ_{LP}, we examined the sensitivity of φ_{LP} to these two parameters, individually and in combination, for all values of P in our data (see Methods). Sensitivity of φ_{LP} to these two parameters varied across P values, with larger sensitivity at lower values of P (Two-Way RM-ANOVA, $p<0.001$,

F=16.054; data included in Figure 7-source data). For simplicity, we averaged the sensitivity values across different *P* values to obtain an overall measure of the influence of g_{max} and Δ_{peak}. These results showed that, for the C-DC case, φ_{LP} had a positive sensitivity to g_{max} and a smaller positive sensitivity to Δ_{peak} (Fig. 7A). The sensitivity was largest if the two parameters were varied together (g_{max} + Δ_{peak}) and smallest if they were varied in opposite directions (g_{max} - Δ_{peak}; Two-Way RM-ANOVA, $p<0.001$, $F=3.330$). Similarly, these sensitivity values were also significantly different for the C-Dur case (Fig. 7B; Two-Way RM-ANOVA, $p<0.001$, $F=2.892$), with largest sensitivity for g_{max} + Δ_{peak} and smallest for g_{max} - Δ_{peak}.

Level sets of φ_{LP} in the P-g_{max}-φ_{peak} space for C-DC and C-Dur cases

To search for phase constancy across different *P* values in our dataset, we expressed φ_{LP} as a function of the three IPSC parameters, *P*, g_{max} and Δ_{peak}: $\varphi_{LP} = \Phi(P, g_{\max}, \Delta_{peak})$. Figure 8 shows heat map plots of the function Φ, plotted for the range of values of *P* and Δ_{peak} and four values of g_{max}. In these plots, phase constancy can be seen as the set of values in each graph that are isochromatic, indicating the level sets of the function Φ. These level sets are mathematically defined as hypersurfaces on which the function has a constant value: $\Phi(P, g_{\max}, \Delta_{peak}) = \varphi_c$. For the C-DC case, in each g_{max} section of the plot, the level sets (e.g. φ_c = 0.34 denoted in white) spanned a moderate range of P values as Δ_{peak} increased (Fig. 8A1). The span of *P* values across all four panels indicates the range of cycle periods for which phase constancy could be achieved by varying g_{max} and Δ_{peak}. This range of *P* values (spanned by the white curves) was considerably smaller for the C-Dur case (Fig. 8A2).

For any constant phase value φ_c, these level sets can be expressed as

$$P = P_{\varphi_c}(g_{\max}, \Delta_{peak}),$$

which describes a surface in the 3D space, yielding the *P* value for which phase can be maintained at φ_c, for the given values of g_{max} and Δ_{peak}. The level set indicated by the white curves in panel A for the C-DC case is plotted as a heat map in Fig. 8B1 and can be compared with the same plot for the C-Dur case in Fig. 8B2. The range of colors in each plot (marked next to each panel) indicates the range of *P* values for which phase can be kept at φ_c = 0.34. To reveal how this range depends on the desired phase, we measured this range for all values of φ_c between 0.2 and 0.8 (Figs. 8C1 and 8C2). We

found that the LP neuron could not achieve phases below 0.3 in the C-DC case (Fig. 8C1), which is simply because the neuron never fired during the inhibitory synaptic current (which had a duty cycle of 0.3). Furthermore, the range of P values for which the LP phase could be maintained by varying g_{max} and Δ_{peak} was much larger for C-DC inputs compared to C-Dur Inputs, for all φ_c values between 0.31 and 0.54.

A model of synaptic dynamics could predict activity onset phase of the LP neuron

To gain a better understanding of our experimental results, we derived a mathematical description of the phase of a follower neuron such as LP, based on the following assumptions: 1, that the firing time of this neuron was completely determined by its synaptic input, 2, that in each cycle the synaptic conductance g_{syn} increased to a maximum value g_{max} for a time interval T_{act} (the active duration of the synapse) and decayed to 0 otherwise, and 3, that the follower neuron remained inactive when g_{syn} was above some threshold g^*. The derivation of this model is described in the Methods.

This simple model provided a mathematical description of φ_{LP} as a function of P, g_{max} and Δ_{peak}, for the C-Dur and C-DC cases. In the C-Dur case (Equation (7)), as P increased, φ_{LP} decayed and approached 0 like $1/P$. In contrast, in the C-DC case (Equation (8)), φ_{LP} approached its lower limit $\Delta_{peak} \cdot DC$, as P increased, and thus behaved very differently than in the C-Dur case.

We used these equations to describe g_{max} as a function of P (for any given Δ_{peak}) so that LP maintained a constant phase φ_c, (Equation (10) for the C-DC case). Alternatively, Δ_{peak} could be given as a function of P (for any given g_{max}, Equation (11) for the C-DC case). We used these derivations to compare how phase constancy depends on g_{max} or Δ_{peak} in the C-DC case. A comparison of these two cases can be seen in Fig. 9A, where either g_{max} (green) or Δ_{peak} (blue) is varied to keep φ_{LP} constant at φ_c=0.34 across different P values. (The red curve is the depressing case, described below.) As the figure shows, phase constancy can be achieved by varying either parameter, but each parameter produces a different range of P across which phase is maintained.

These equations and their corresponding counterparts for the C-Dur case can be used to calculate the range of P values over which changing Δ_{peak} (from 0 to 1) can maintain a constant phase φ_c. If ΔP denotes the range of P values for which phase can

be constant, it is straightforward to show that $\Delta P_{DC} > \Delta P_{Dur}$ (compare black and blue curves in Fig. 9B and 9C; see Methods for derivation).

Two additional points are notable in Fig. 9C. First, the lower bound on φ_{LP} for which phase constancy can occur is smaller in the C-Dur than the C-DC case. This is because we have assumed that in the C-DC case the LP neuron cannot fire during inhibition (i.e., until after Δ_{peak} *DC*). Second, for φ_c larger than ~ 0.5, ΔP is larger for the C-Dur case. This occurs because Equation (12) can no longer be satisfied when φ_c is large. That is, with constant duty cycle, it is not possible to produce an arbitrarily large follower neuron phase, but with constant duration, any large phase is attainable if the cycle period is not much larger than the synaptic duration. These findings are consistent with our experimental results described above (see Fig. 8).

The pacemaker synaptic input to the LP neuron shows short-term synaptic depression (Rabbah and Nadim, 2007). In a previous modeling study, we explored how the phase of a follower neuron was affected when the inhibitory synapse from an oscillatory neuron to this follower had short-term synaptic depression (Manor et al., 2003). In that study the role of the parameter Δ_{peak} was not considered. We now consider how the presence of short-term synaptic depression influences phase constancy by changing both g_{max} and Δ_{peak}. As stated in the Methods (Equation (16)), the effect of synaptic depression on synaptic strength can be obtained as $g_{max} = \bar{g}_{max} \cdot s_{max}(P)$), where s_{max} is an increasing function whose value approaches 1 as *P* increases. This indicates that the synapse becomes stronger due to more recovery from depression at longer cycle periods. When synaptic depression dictates how g_{max} varies with *P* and Δ_{peak} also varies with *P* and g_{max} (Equation (11)), the simultaneous changes in g_{max} and Δ_{peak} (red) greatly increase the range of *P* values over which φ_{LP} is constant (Fig. 9A).

Note that the C-DC case with short-term depression spans a larger range of *P* values than the non-depressing case (Fig. 9B). Similarly, the range of *P* values for which phase can be maintained is larger than the non-depressing case across φ_{LP} values, except where φ_{LP} is so large that the depressing synapse operates outside its dynamic range (Fig. 9C). These results are consistent with our experimental results, indicating that although phase constancy can be achieved when either g_{max} or Δ_{peak} increases with *P*, a concomitant increase of both - which could occur for example with

a depressing synapse - greatly expands the range of *P* values for which a constant phase is maintained.

Discussion

The importance of phase in oscillatory networks

A common feature of oscillatory networks is that the activities of different neuron types are restricted to specific phases of the oscillation cycle. For example, different hippocampal and cortical neurons are active in at least three distinct phases of the gamma rhythm (Hajos et al., 2004; Hasenstaub et al., 2005), and distinct hippocampal neuron types fire at different phases of the theta rhythm and sharp wave-associated ripple episodes (Somogyi and Klausberger, 2005).

Experimental studies quantify the latency of neural activity with respect to a reference time in the cycle, but in most cases, these latencies are normalized and reported as phase. Distinct neuron types can maintain a coherent activity phase, despite wide variations in the network frequency (30-100 Hz for gamma rhythms, 4-7 Hz for theta rhythms, and 120-200 Hz for sharp wave-associated ripple episodes). Phase-specific activity of different neuron types is proposed to be important in rhythm generation (Wang, 2010), and indicates the necessity of precise timing for producing proper circuit output and behavior (Kopell et al., 2011). For example, phase locking of spike patterns to oscillations is important for auditory processing, single cell and network computations and Hebbian learning rules (Kayser et al., 2009; McLelland and Paulsen, 2009; Panzeri et al., 2010). For brain oscillations, phase relationships may provide clues about the underlying circuit connectivity and dynamics, but a behavioral correlate of varying frequencies is not obvious. In contrast, the activity phase of distinct neuron types in rhythmic motor circuits is a tangible readout of the timing of motor neurons and muscle contractions, thus defining phases of movement (Grillner and El Manira, 2015; Kiehn, 2016; Le Gal et al., 2017; Bidaye et al., 2018). Because meaningful behavior depends crucially on proper activity phases, whether neurons maintain their activity phase in face of changes in frequency simply translates to whether the movement pattern changes as it speeds up or slows down.

Determinants of phase

In oscillatory networks, the activity phases of different neuron types depend to different degrees on the precise timing and strength of their synaptic inputs (Oren et

al., 2006). Our results from noise current injections showed that the timing of the LP neuron is strongly dependent on the timing of inputs it receives. Dynamic clamp injection of realistic or triangular conductance waveforms with different periods (*P*) indicated that φ_{LP} was largely determined by the duration of the synaptic input. φ_{LP} changed substantially with *P* when inputs had constant duration, but much less when inputs had a constant duty cycle, i.e., when duration scaled with *P*. However, our experiments also showed that inputs of constant duty cycles alone are insufficient for phase constancy. φ_{LP} decreased with *P* even with a constant duty cycle of inputs, but increased with either synaptic strength (g_{max}) or peak phase of the synaptic input (Δ_{peak}). The increase in φ_{LP} had similar sensitivity to g_{max} and Δ_{peak}, and therefore a larger sensitivity to a simultaneous increase in both. Consequently, it was possible to keep φ_{LP} constant over a wide range of cycle periods by increasing both parameters with *P*.

The fact that an increase in g_{max} with *P* promotes phase constancy is biologically relevant, as short-term depression in pyloric synapses means that synaptic strength indeed increases with *P* (Manor et al., 1997). Previous modeling studies show that short-term synaptic depression of inhibitory synapses promotes phase constancy (Nadim et al., 2003; Bose et al., 2004), largely because of longer recovery times from depression at larger values of *P*.

The finding that an increase of Δ_{peak} with *P* promotes phase maintenance is somewhat surprising, as we have previously shown that Δ_{peak} in LP actually decreases with *P* (Manor et al., 1997; Tseng et al., 2014). On the face of it, this suggests that an increase in Δ_{peak} is not a strategy employed in the intact circuit. However, the caveat is that such results may critically depend on the cause of the change in *P,* either technically and biologically. While in our current study we varied Δ_{peak} with direct conductance injection into LP, previous results were obtained by changing the waveform and period of the presynaptic pacemaker neurons. When *P* is changed in an individual preparation by injecting current into or voltage-clamping the pacemakers, phase of follower neurons is not particularly well maintained. An example of this is shown in Fig. 1, where φ_{LP} values fall between constant phase and constant duration and, additionally, all pyloric neurons show behavior that falls between constant phase and constant latencies (Hooper, 1997b, a). This may reflect that neurons are not keeping phase particularly well when the only cause of changing *P* is the presynaptic

404 input. This is supported by the observation that even during normal ongoing pyloric
405 activity, phases change with cycle-to-cycle variability of P in individual preparations
406 (Bucher et al., 2005). However, it does not preclude the possibility that Δ_{peak} plays an
407 important role in stable phase relationships when P differs because of temperature,
408 neuromodulatory conditions, or inter-individual variability (discussed below).

409 It is noteworthy that a change in the synaptic strength or peak phase with P is
410 not peculiar to graded synapses. The fact that short-term synaptic plasticity can act as
411 a frequency-dependent gain control mechanism is well known for many spike-mediated
412 synaptic connections. In bursting neurons, the presence of a combination of short-term
413 depression and facilitation in the same spike-mediated synaptic interaction could also
414 result in changes in the peak phase of the summated synaptic current as a function of
415 burst frequency and duration, and the intra-burst spike rate (Markram et al., 1998).

416 The mathematical model in the current study provides mechanistic explanations
417 for several of our experimental findings. First, it can be used to produce a quantitative
418 measure of phase, given the values of g_{max}, Δ_{peak} and P. Thus, these equations can be
419 used to compare the C-DC and C-Dur cases, which match our experimental results.
420 They show that, for most phase values, the C-DC case provides a larger range of cycle
421 periods at which phase constancy can occur. Second, these equations provide the
422 activity phase no matter how the pacemaker synaptic input duration changes with cycle
423 period. For instance, our experiments were conducted by changing synaptic input
424 through sampling individual values of the parameter pairs g_{max} and Δ_{peak}, and then
425 calculating the ensuing phase. We then used fitting to find level sets of constant phase
426 (Fig. 8). In contrast, when we combined our mathematical derivation here with previous
427 results on the role of short-term synaptic depression (Bose et al., 2004), we could
428 demonstrate how a neuronal circuit can naturally follow a level set of phase (Equations
429 (7), (8), (15) and (16)). Moreover, we showed that the combined increase in g_{max} and
430 Δ_{peak} with P produces a larger range of periods for phase constancy than increasing
431 either parameter alone. In short, this mathematical formulation produces a simple
432 quantitative distillation of our experimental results.

433 In this study, we did not explore the role of the intrinsic properties of the LP
434 neuron on its phase. In separate experiments, we simultaneously measured post-
435 inhibitory rebound properties in synaptically isolated LP neurons and the levels of
436 voltage-gated ionic currents (the transient potassium current I_A and the

hyperpolarization-activated inward current I_h) that influence rebound spiking. These data were not included in this study for brevity and because they showed that the timing of post-inhibitory spiking was relatively stable across preparations. Therefore, we would expect the contribution of intrinsic properties in controlling the timing of the LP neuron burst onset to be relatively small. However, this result does not generalize to all follower neurons. For example, the follower ventral dilator (VD) and PY neurons have a much higher levels of I_A, which in turn has a larger effect on the timing of post-inhibitory spiking. In a set of computational studies, we addressed the role of I_A in determining the burst phase in response to periodic inputs (Zhang et al., 2008, 2009) and in conjunction with short-term depression in the synaptic input (Bose et al., 2004). An experimental clarification of the relative contribution of intrinsic properties vs. synaptic input could be done with controlled dynamic clamp synaptic input, such as those used in the current study, injected in PY or VD neurons. Such a data set would fittingly complement the results of the current study to elucidate more general rules in determining the activity phase of neurons in an oscillatory network.

Phase relationships in changing temperatures

An interesting case is provided by the observation that phases are remarkably constant when pyloric rhythm frequency is changed with temperature. Tang et al. (2012) report a 4-fold decrease in P of the pyloric rhythm between 7 and 23° C. In this study, none of the pyloric phases changed significantly, and it is worth noting that under conditions of changing temperatures, the relationships between P, g_{max}, and Δ_{peak} appeared to be fundamentally different from when P is changed at a constant temperature. Presynaptic voltage trajectories scaled with changing P, and Δ_{peak} of postsynaptic currents was independent of P, in contrast to the decrease described at constant temperature (Manor et al., 1997; Tseng et al., 2014). Amplitudes of synaptic potentials did not change with temperature, despite an increase in synaptic current amplitudes with increasing temperature (and associated decrease in P). This is in contrast to the positive relationship between g_{max} and P that results from synaptic depression at a constant temperature (Manor et al., 1997). Therefore, it appears that the likely substantial effects of temperature on synaptic dynamics and ion channel gating are subject to a set of compensatory adaptations different from when P is changed at constant temperature.

Variability and slow compensatory regulation of phase

Phase maintenance in the face of changing *P* in an individual animal requires the appropriate short-term dynamics of synaptic and intrinsic neuronal properties. The fact that characteristic (and therefore similar) phase relationships can also be observed under the same experimental conditions across individual preparations is a different conundrum, particularly when *P* can vary substantially, as is true for brain oscillations (Hajos et al., 2004; Hasenstaub et al., 2005; Somogyi and Klausberger, 2005). Phases show different degrees of variability across individuals in a variety of systems, e.g., leech heartbeat (Wenning et al., 2018), larval crawling in *Drosophila* (Pulver et al., 2015), and fictive swimming in zebrafish (Masino and Fetcho, 2005), but in all of these cases phases are not correlated with *P*. In the pyloric rhythm, phases are also variable to a degree across individuals, but not correlated with the mean *P*, which varies >2-fold (Bucher et al., 2005; Goaillard et al., 2009). This phase constancy occurs despite considerable inter-individual variability in ionic currents, and is considered the ultimate target of slow compensatory regulation, i.e., homeostatic plasticity (Marder and Goaillard, 2006; Ma and LaMotte, 2007; Marder et al., 2014). Slow compensation can also be observed directly when rhythmic activity is disrupted by decentralization, and subsequently recovers to similar phase relationships over the course of many hours (Luther et al., 2003). It is interesting to speculate if our findings about how synaptic parameters must change to keep phase constant would hold across individuals with different mean *P*. The prediction would be coordinated positive correlations of both g_{max} and Δ_{peak} with *P*.

Synaptic inputs to the LP neuron show considerable variability across preparations (e.g., Fig. 3B), which mirrors the variability seen in the levels of voltage-gated ionic currents in pyloric neurons (Schulz et al., 2006). We did not address the role and extent of variability in this study, because a proper analysis of variability required us to first establish the mechanisms that give rise to a consistent output, in this case phase constancy. Based on our findings regarding the influence of synaptic parameters on phase, a natural next step is to explore whether the variability of different parameters defining the synaptic input influences variability of phase or, alternatively, whether variability in some synaptic parameters may be irrelevant to phase or restrained by the postsynaptic neuron.

Phase relationships under different neuromodulatory conditions.

The flipside of the question how neurons maintain phase is the question how their phase can be changed. In motor systems in particular, changes in phase relationships are functionally important to produce qualitatively different versions of circuit output, for example to produce different gaits in locomotion (Vidal-Gadea et al., 2011; Grillner and El Manira, 2015; Kiehn, 2016). The activity of neural circuits is flexible, and much of this flexibility is provided by modulatory transmitters and hormones which alter synaptic and intrinsic neuronal properties (Brezina, 2010; Harris-Warrick, 2011; Jordan and Slawinska, 2011; Bargmann, 2012; Marder, 2012; Bucher and Marder, 2013; Nadim and Bucher, 2014). The pyloric circuit is sensitive to a plethora of small molecule transmitters and neuropeptides which affect cycle frequency and phase relationships (Marder and Bucher, 2007; Stein, 2009; Daur et al., 2016). Indeed, extensive research has indicated the role of amine modulation of synaptic strength and neuronal firing phase in the pyloric circuit, and how amine modulation of synaptic and intrinsic firing properties changes firing phases (Johnson et al., 2003; Gruhn et al., 2005; Johnson et al., 2005; Peck et al., 2006; Harris-Warrick and Johnson, 2010; Harris-Warrick, 2011; Kvarta et al., 2012). With respect to our findings, any given neuromodulator could act presynaptically to alter *P*, duration, or duty cycle on the one hand, and g_{max} and Δ_{peak} on the other. In addition, the neuromodulator could affect the postsynaptic neuron's properties and alter its sensitivity to any of these parameters. Therefore, our findings could not just further our understanding of how phase can be maintained across different rhythm frequencies, but also provide a framework for testing if and how changes in synaptic dynamics may contribute to altering phase relationships under different neuromodulatory conditions.

Materials and Methods

Adult male crabs (*Cancer borealis*) were acquired from local distributors and maintained in aquaria filled with chilled (10-13°C) artificial sea water until use. Crabs were prepared for dissection by placing them on ice for 30 minutes. The dissection was performed using standard protocols as previously described (Tohidi and Nadim, 2009; Tseng and Nadim, 2010). The STNS, including the four ganglia (esophageal ganglion, two commissural ganglia, and the STG) and their connecting nerves, and the motor nerves arising from the STG, were dissected from the stomach and pinned into a Sylgard (Dow-Corning) lined Petri dish filled with chilled saline. The STG was desheathed, exposing the somata of the neurons for intracellular impalement.

Preparations were superfused with chilled (10-13°C) physiological *Cancer* saline containing: 11 mM KCl, 440 mM NaCl, 13 mM $CaCl_2 \cdot 2H_2O$, 26 mM $MgCl_2 \cdot 6H_2O$, 11.2 mM Trizma base, 5.1 mM maleic acid with a pH of 7.4.

Extracellular recordings were obtained from identified motor nerves using stainless steel electrodes, amplified using a differential AC amplifier (A-M Systems, model 1700). One lead was placed inside a petroleum jelly well created to electrically isolate a small section of the nerve, the other right outside of it. For intracellular recordings, glass microelectrodes were prepared using the Flaming-Brown micropipette puller (P97; Sutter Instruments) and filled with 0.6 M K_2SO_4 and 20 mM KCl. Microelectrodes used for membrane potential recordings had resistances of 25-30MΩ; those used for current injections had resistances of 15-22 MΩ. Intracellular recordings were performed using Axoclamp 2B and 900A amplifiers (Molecular Devices). Data were acquired using pClamp 10 software (Molecular Devices) and the Netsuite software (Gotham Scientific), sampled at 4-5 kHz and saved on a PC using a Digidata 1332A (Molecular Devices) or a PCI-6070-E data acquisition board (National Instruments).

Individual pyloric neurons were impaled and identified via their membrane potential waveforms, correspondence of spike patterns with extracellular nerve recordings, and interactions with other neurons within the network (Weimann et al., 1991).

Constructing realistic graded IPSC waveforms

Inhibitory postsynaptic currents (IPSCs) were recorded from LP neurons during the ongoing rhythm using two-electrode voltage clamp and holding the LP neuron at -50mV, far from the IPSC reversal potential of ~ -80 mV (Fig. 3A). We refer to the total current measured in the voltage clamped LP neuron during the activity of the PD and PY neurons as a synaptic current for the following reasons: 1, the synaptically isolated LP neuron produces tonic spiking activity (see, e.g., Fig. 2B), and 2, holding the LP neuron at different voltages (e.g. -60 or -110 mV) produces a similarly shaped current, but with a different amplitude or reversed sign (at -110 mV).

When the LP soma is voltage clamped at -50 mV, the axon (which is electrotonically distant from the soma) produced action potentials following the synaptic inhibition from the PY neuron and the pacemaker neurons. The onset of the LP neuron

action potentials (recorded in the current trace) was used to calculate the mean IPSC for each experiment averaging the IPSCs over 10-20 cycles. The IPSC waveforms were then extracted by normalizing both the amplitude and the duration of the mean IPSC.

Driving the LP neuron with noise current

In these experiments, the preparation was superfused in *Cancer* saline plus 10^{-5} M picrotoxin (PTX; Sigma Aldrich) for 30 minutes to block the synaptic currents to the LP neuron. The removal of synaptic inhibition onto LP neurons changed the activity of these neurons from bursting to tonic firing. Then, noise current, generated by the Ornstein-Uhlenbeck (O-U) process (Lindner), was injected into the LP neurons for 60 minutes using the Scope software (available at http://stg.rutgers.edu/Resources.html, developed in the Nadim laboratory). The baseline of the noise current was adjusted by adding DC current so that it can provide enough inhibition to produce silent periods alternating with bursts of action potentials. The O-U process was defined as

$$dX_t = -\frac{1}{\tau} X_t dt + \sigma dW_t.$$

The parameters used for noise injection were τ =10 to 20 ms, σ = 200 pA and a DC current of -200 to -100 pA. In these experiments we defined bursts as groups of at least two action potentials with inter-spike intervals < 300 ms, following a gap of at least 300 ms.

Driving the LP neuron with realistic or triangular IPSC waveforms in dynamic clamp

The dynamic clamp current was injected using the Netclamp software (Netsuite, Gotham Scientific). We pharmacologically blocked synaptic inputs from the pacemaker AB and follower PY neurons to the LP neuron by superfusing the perparation in *Cancer* saline plus 10^{-5} M picrotoxin (PTX; Sigma Aldrich) for 30 minutes. This treatment does not block the cholinergic synaptic input from the PD neurons for which no clean pharmacological blocker is known. Although the PD neuron input has some influence on the LP neuron activity, this input only constitutes <20% of the total pacemaker synapse and cannot drive oscillations in the follower LP neuron.

The LP neuron was driven in PTX with an artificial synaptic current in dynamic clamp. The synaptic current was given as

$$I_{syn} = g_{syn}(V_{LP} - E_{syn})$$

where the synaptic conductance g_{syn} was a pre-determined waveform, repeated periodically with period P, and E_{syn} was the synaptic reversal potential set to −80 mV (Zhao et al., 2011).

Two sets of dynamic clamp experiments were performed on different animals. In one set of experiments, g_{syn} was set to be a triangular waveform. We measured the effects of four different parameters in these triangle conductance injections (Fig. 1): peak phase (Δ_{peak}), duration (T_{act}), period (P = time between onsets of dynamic clamp synaptic injections), and maximal conductance (g_{max}, the peak value of g_{syn}). This allowed us to explore which combinations of the different parameters influences the LP phase. Five values for P were used: 500, 750, 1000, 1500, and 2000 ms, which cover the typical range of pyloric cycle periods. Three values of g_{max} were used: 0.1, 0.2 and 0.4 μS, consistent with previous measurements of synaptic conductance (Zhao et al., 2011; Tseng et al., 2014). The value of Δ_{peak} was varied to be 0, 0.25, 0.5, 0.75 or 1. In the same experiment, all runs were done in two conditions: with T_{act} constant across different P values (C-Dur case with T_{act} = 300 ms) or with T_{act} changing proportionally to P (C-DC case with duty cycle $DC = T_{act}/P = 0.3$).

In the other set of experiments, g_{syn} was a realistic IPSC waveform, based on a pre-recorded IPSC in the LP neuron. In these experiments, P was varied to be 500, 750, 1000, 1250, 1500, or 2000 ms by scaling the realistic waveform in the time direction. In these experiments, g_{max} was set to be 0.1, 0.2, 0.4, 0.6, or 0.8 μS. The LP neuron burst onset delay (Δt) was measured relative to the onset of the pacemaker component of the synaptic input (identified by the kink in the synaptic conductance waveform) in each cycle. The burst phase was calculated as $\varphi_{LP} = \Delta t/P$. Phase constancy means that Δt changed proportionally to P. To measure the LP neuron phase with respect to the end of the pacemaker input, this reference used was the point on the synaptic conductance waveform marked by drawing a horizontal line from the kink that identified the onset of the pacemaker input.

626 *Determining relationship between cycle period (P), synaptic strength (g_{max}) and LP*
627 *phase (φ_{LP}) using the realistic IPSC waveform*

628 We determined how well the mathematical model derived for constant input
629 duty cycles (see Equation (8) below), matched the experimental data obtained with
630 realistic IPSC waveforms. To this end, we fit the model to φ_{LP} values measured for all
631 values of g_{max} and P, using the standard fitting routine 'fit' in MATLAB (Mathworks).

632 *Sensitivity of φ_{LP} to g_{max} and Δ_{peak} across all P values*

633 To explore how g_{max} and Δ_{peak} may interact to influence φ_{LP}, we examined the
634 sensitivity of φ_{LP} to these two parameters, individually and in combination, for all values
635 of P in our data. For each P, we computed the mean value of φ_{LP} across all
636 experiments, and all values of g_{max} (0.1, 0.2, 0.3 and 0.4 µS) and Δ_{peak} (0, 0.25, 0.5,
637 0.75 or 1). (The φ_{LP} value for g_{max} = 0.3 µS was obtained in this case by linearly
638 interpolating the values for 0.2 and 0.4 µS.) This produced a 4 by 5 matrix of all values.
639 For each data point in the matrix, we moved along eight directions ($+g_{max}$, $+\Delta_{peak}$, $-g_{max}$,
640 $-\Delta_{peak}$, $+g_{max}$ & $+\Delta_{peak}$, $-g_{max}$ & $-\Delta_{peak}$, $+g_{max}$ & $-\Delta_{peak}$, $+g_{max}$ & $-\Delta_{peak}$). Here "+" denotes
641 increasing and "-" denotes decreasing. We then calculated the change in φ_{LP} per unit
642 g_{max} (normalized by 0.4 µS), Δ_{peak}, or both. For example, the sensitivity of φ_{LP} when
643 Δ_{peak} was changed from 0.25 to 0.5 was measured as

644 $$\frac{\varphi_{LP}(\text{at } \Delta_{peak} = 0.5) - \varphi_{LP}(\text{at } \Delta_{peak} = 0.5)}{0.5 - 0.25}$$

645 Similarly, the sensitivity of φ_{LP} when g_{max} was changed from 0.2 to 0.4 was measured
646 as

647 $$\frac{\varphi_{LP}(\text{at } g_{\max} = 0.4) - \varphi_{LP}(\text{at } g_{\max} = 0.2)}{(0.4 - 0.2)/0.4}$$

648 These data are provided in Figure 7-source data. As the next step, we averaged the
649 sensitivity along each aligned direction: [$+g_{max}$ and $-g_{max}$]; [$+\Delta_{peak}$ and $-\Delta_{peak}$]; [$+g_{max}$ &
650 $+\Delta_{peak}$ and $-g_{max}$ & $-\Delta_{peak}$]; [$+g_{max}$ & $-\Delta_{peak}$ and $+g_{max}$ & $-\Delta_{peak}$]. This produced the four
651 cardinal directions, shown in Fig. 7. Finally, we averaged the sensitivity across all P
652 values.

653 *A model of synaptic dynamics*

In the derivation of the model, the firing time of the LP neuron was assumed to be completely determined by its synaptic input. This synaptic conductance (g_{syn}) was assumed to rise and fall with distinct time constants. The following holds over one cycle period and therefore time is reset with period P (t (mod P)):

$$\frac{dg_{syn}}{dt} = \begin{cases} (g_{\max} - g_{syn})\tau_r & t \ (\mathrm{mod} P) < t_{peak} \\ -g_{syn} / \tau_s & t \ (\mathrm{mod} P) \geq t_{peak} \end{cases} \quad (1)$$

where the time t_{peak}, corresponding to Δ_{peak}, is $t_{peak} = \Delta_{peak} T_{act}$. We assumed that LP neuron remained inactive when g_{syn} was above a fixed threshold (g^*) less than g_{max}. Because the synaptic input is periodic with period P, we solved for the minimum and maximum values of g_{syn} in each cycle. The minimum (g_{lo}) occurred just before the onset (t = 0) of AB/PD activity, whereas the maximum occurred at the peak synaptic phase Δ_{peak} for the C-Dur case. In the C-DC case, $T_{act} = DC \cdot P$, where DC is the duty cycle (fixed at 0.3 in our experiments).

To calculate g^*, we set the value t = 0 so that $g_{syn}(0) = g_{lo}$ (and, by periodicity, $g_{syn}(P) = g_{lo}$), and solved the first part of Equation (1) where g_{syn} increases until $t = t_{peak}$. This yielded

$$g_{peak} = g_{syn}(t_{peak}) = g_{max} + (g_{lo} - g_{max})e^{-t_{peak}/\tau_r} \quad (2)$$

We then used the second part of Equation (1) to track the decay of g_{syn} for $t_{peak} < t < P$:

$$g_{syn}(t) = g_{peak} e^{-(t - t_{peak})/\tau_s} \quad (3)$$

Using Equation (3), we calculated the time Δt at which the synaptic conductance $g_{syn}(\Delta t) = g^*$ as follows:

$$g^* = g_{peak} e^{-(\Delta t - t_{peak})/\tau_s} \quad (4)$$

Solving Equation (4) for Δt yielded

$$\Delta t = \tau_s \ln \frac{g(t_{peak})}{g^*} + t_{peak}.$$

Dividing this equation by P yielded φ_{LP}:

678 $$\varphi_{LP} = F(P, g_{max}, \Delta_{peak}) = \frac{\tau_s}{P} \ln \frac{g_{peak}}{g^*} + \frac{t_{peak}}{P}, \quad (5)$$

679 where g_{peak} is given by Equation (2). This expression provides a description of the
680 dependence of φ_{LP} as a function of P, g_{max} and Δ_{peak}. To explore the role of the
681 parameters in this relationship, we made a simplifying assumption that the synaptic
682 conductance $g_{syn}(t)$ rapidly reached its peak (i.e., τ_r was small), stayed at this value and
683 started to decay at $t = t_{peak}$. In this case $g(t) = g_{max}$ on the interval $(0, t_{peak})$ and the value
684 of g_{lo} is irrelevant. With this assumption, Equation (5) reduced to

685 $$\varphi_{LP} = \frac{\tau_s}{P} \ln \frac{g_{max}}{g^*} + \frac{t_{peak}}{P}. \quad (6)$$

686 Substituting $t_{peak} = \Delta_{peak} \cdot T_{act}$ in Equation (6), gave

687 $$\varphi_{LP} = F(P, g_{max}, \Delta_{peak}) = \frac{1}{P}\left(\tau_s \ln \frac{g_{max}}{g^*} + \Delta_{peak} T_{act} \right), \quad (7)$$

688 which we used to describe the LP phase in the C-Dur case. To describe the C-DC
689 case, after substituting $t_{peak} = \Delta_{peak} \cdot DC \cdot P$, we obtained

690 $$\varphi_{LP} = F(P, g_{max}, \Delta_{peak}) = \frac{1}{P}\left(\tau_s \ln \frac{g_{max}}{g^*} \right) + \Delta_{peak} DC. \quad (8)$$

691 Note that these equations also describe the relationship between φ_{LP} with T_{act} in the C-
692 Dur case, and DC in the C-DC case).

693 Equations (7) and (8) can be used to approximate a range of parameters over
694 which φ_{LP} is maintained at a constant value φ_c. To do so, we assumed a specific
695 parameter set, say $(\hat{P}, \hat{g}_{max}, \hat{\Delta}_{peak})$, satisfies

696 $$F(\hat{P}, \hat{g}_{max}, \hat{\Delta}_{peak}) = \varphi_c,$$

697 for some fixed phase value, φ_c. We could now ask whether there are nearby
698 parameters for which phase remains constant, i.e., F remains equal to φ_c. The Implicit
699 Function Theorem (Krantz and Parks, 2012) guarantees that this is the case, provided
700 certain derivatives evaluated at $(\hat{P}, \hat{g}_{max}, \hat{\Delta}_{peak})$ are non-zero, which turns out to be true

over a large range of parameters. Since the partial derivative with respect to Δ_{peak} of $F(P,g_{max},\Delta_{peak})$ at this point is a non-zero constant equal to T_{act}/P (or DC) in the C-Dur (or C-DC) case, there is a function $\Delta_{peak} = h(P,g_{max})$ such that

$$F(P,g_{max},h(P,g_{max})) = \varphi_c \tag{9}$$

for values of P and g_{max} near $(\hat{P},\hat{g}_{max})$. In other words, the Implicit Function Theorem guarantees that small changes in P and g_{max} can be compensated for by an appropriate choice of Δ_{peak} in order to maintain a constant LP phase. A similar analysis can be done by solving for g_{max} in terms of P and Δ_{peak} or by solving for P in terms of g_{max} and Δ_{peak}.

Keeping g_{max} (respectively, Δ_{peak}) constant in these equations allows us to obtain a relationship between P and Δ_{peak} (respectively, g_{max}), for which φ_{LP} is kept constant at φ_c. Consider Equations (7) and (8) for fixed values of both φ_{LP} (= φ_c) and g_{max}. Then these equations reduce to simple functional relationships where Δ_{peak} can be expressed as a function of P. In the C-DC case, for example, evaluating Δ_{peak} from Equation (8) produces

$$g_{max} = g^* \cdot \exp\left(\frac{P}{\tau_s}(\varphi_c - \Delta_{peak} DC)\right) \tag{10}$$

Equation (10) describes how g_{max} must vary with P for the system to maintain a constant phase φ_c for any given Δ_{peak}.

Alternatively, Δ_{peak} can be expressed as a function of P. In the C-DC case, evaluating Δ_{peak} from Equation (8) produces

$$\Delta_{peak} = \frac{\varphi_c}{DC} - \frac{\tau_s}{DC \cdot P}\ln\frac{g_{max}}{g^*}, \tag{11}$$

Equation (11) can be used to calculate the range of P values over which changing Δ_{peak} (from 0 to 1) can maintain a constant phase φ_c. Solving $0 < \Delta_{peak} < 1$ using Equation (11) yields

$$\frac{\tau_s}{\varphi_c}\ln\frac{g_{max}}{g^*} < P_{DC} < \frac{\tau_s}{\varphi_c - DC}\ln\frac{g_{max}}{g^*} \tag{12}$$

Performing the same procedure in the C-Dur case, we find

$$\frac{\tau_s}{\varphi_c}\ln\frac{g_{max}}{g^*} < P_{Dur} < \frac{T_{act}}{\varphi_c} + \frac{\tau_s}{\varphi_c}\ln\frac{g_{max}}{g^*}. \quad (13)$$

The lower limits of the two cases (P_{DC} and P_{Dur}) are the same. The upper limit for P_{DC} is larger than that of P_{Dur} if

$$\varphi_c < DC\left(1 + \frac{\tau_s}{T_{act}}\ln\frac{g_{max}}{g^*}\right). \quad (14)$$

If ΔP denotes the range of P values that respectively satisfy Equation (12) or (13), then $\Delta P_{DC} > \Delta P_{Dur}$ if the inequality given by (14) holds, which it does for true for τ_s and g_{max} large enough.

Adding synaptic depression to the model of synaptic dynamics

In a previous modeling study, we explored how the phase of a follower neuron was affected when the inhibitory synapse from an oscillatory neuron to this follower had short-term synaptic depression (Manor et al., 2003). In that study the role of the parameter Δ_{peak} was not considered. It is straightforward to add synaptic depression to Equations (7) and (8) and therefore examine how phase is affected if Δ_{peak} increases with P and synaptic strength also changes with P according to the rules of synaptic depression. We will restrict this section to the C-DC case. A similar derivation can be made for the C-Dur case.

An *ad hoc* model of synaptic depression can be made using a single variable s_d which will be a periodic function that denotes the extent of depression and takes on values between 0 and 1 (Bose et al., 2004). s_d decays during the AB/PD burst (from time 0 to T_{act}, indicating depression) and then recovers during the inter-burst interval (from T_{act} to P, indicating recovery). Thus, s_d can be described by an equation of the form:

$$\frac{ds_d}{dt} = \begin{cases} -s_d/\tau_\beta & t \pmod P \le T_{act} \\ (1-s_d)/\tau_\alpha & T_{act} < t \pmod P < P \end{cases}$$

Using periodicity, it is straightforward to show that the maximum value of s_d, which occurs at the start of the AB/PD burst, is given by:

$$s_{max}(P) = \frac{1 - e^{-P(1-DC)/\tau_\alpha}}{1 - e^{-P(1-DC)/\tau_\alpha} e^{-DC \cdot P/\tau_\beta}}. \quad (15)$$

Note that s_{max} is a monotonically increasing function with values between 0 and 1. Its value approaches 1 as P increases, indicating that the synapse becomes stronger. For a complete derivation and description, see (Bose et al., 2004). The effect of synaptic depression on synaptic strength can be obtained by setting

$$g_{max} = \bar{g}_{max} \cdot s_{max}(P) \quad (16)$$

where s_{max} is given by Equation (15).

Software, analysis and statistics

Data were analyzed using MATLAB scripts to calculate the time of burst onset and the phase. Statistical analysis was performed using Sigmaplot 12.0 (Systat). Significance was evaluated with an α value of 0.05, error bars and error values reported denote standard error of the mean (SEM).

Acknowledgements

We thank Drs. Horacio Rotstein and Eric Fortune for helping with the initial MATLAB scripts in the analysis. This study was supported by NIH MH060605 and NSF DMS1122291.

Competing interests

The authors declare no competing financial interests.

References

Bargmann CI (2012) Beyond the connectome: how neuromodulators shape neural circuits. Bioessays 34:458-465.

Belluscio MA, Mizuseki K, Schmidt R, Kempter R, Buzsaki G (2012) Cross-frequency phase-phase coupling between theta and gamma oscillations in the hippocampus. J Neurosci 32:423-435.

Bidaye SS, Bockemuhl T, Buschges A (2018) Six-legged walking in insects: how CPGs, peripheral feedback, and descending signals generate coordinated and adaptive motor rhythms. J Neurophysiol 119:459-475.

Bose A, Manor Y, Nadim F (2004) The activity phase of postsynaptic neurons in a simplified rhythmic network. J Comput Neurosci 17:245-261.

781 Brezina V (2010) Beyond the wiring diagram: signalling through complex
782 neuromodulator networks. Philos Trans R Soc Lond B Biol Sci 365:2363-
783 2374.
784 Bucher D, Marder E (2013) SnapShot: Neuromodulation. Cell 155:482-482 e481.
785 Bucher D, Prinz AA, Marder E (2005) Animal-to-animal variability in motor pattern
786 production in adults and during growth. J Neurosci 25:1611-1619.
787 Bucher D, Haspel G, Golowasch J, Nadim F (2015) Central Pattern Generators. eLS.
788 Buzsaki G, Wang XJ (2012) Mechanisms of gamma oscillations. Annu Rev Neurosci
789 35:203-225.
790 Buzsaki G, Tingley D (2018) Space and Time: The Hippocampus as a Sequence
791 Generator. Trends in cognitive sciences 22:853-869.
792 Cohen AH, Ermentrout GB, Kiemel T, Kopell N, Sigvardt KA, Williams TL (1992)
793 Modeling of Intersegmental Coordination in the Lamprey Central Pattern
794 Generator for Locomotion. Trends in Neurosciences 15:434-438.
795 Daur N, Nadim F, Bucher D (2016) The complexity of small circuits: the
796 stomatogastric nervous system. Curr Opin Neurobiol 41:1-7.
797 Dicaprio R, Jordan G, Hampton T (1997) Maintenance of motor pattern phase
798 relationships in the ventilatory system of the crab. J Exp Biol 200:963-974.
799 Eisen JS, Marder E (1984) A mechanism for production of phase shifts in a pattern
800 generator. J Neurophysiol 51:1375-1393.
801 Fortune ES, Rose GJ (2001) Short-term synaptic plasticity as a temporal filter.
802 Trends Neurosci 24:381-385.
803 Goaillard JM, Taylor AL, Schulz DJ, Marder E (2009) Functional consequences of
804 animal-to-animal variation in circuit parameters. Nat Neurosci 12:1424-
805 1430.
806 Grande LA, Spain WJ (2005) Synaptic depression as a timing device. Physiology
807 (Bethesda, Md) 20:201-210.
808 Graubard K, Raper JA, Hartline DK (1980) Graded synaptic transmission between
809 spiking neurons. Proc Natl Acad Sci U S A 77:3733-3735.
810 Greenberg I, Manor Y (2005) Synaptic depression in conjunction with A-current
811 channels promote phase constancy in a rhythmic network. J Neurophysiol
812 93:656-677.
813 Grillner S (2006) Biological pattern generation: the cellular and computational logic
814 of networks in motion. Neuron 52:751-766.
815 Grillner S, El Manira A (2015) The intrinsic operation of the networks that make us
816 locomote. Curr Opin Neurobiol 31:244-249.
817 Gruhn M, Guckenheimer J, Land B, Harris-Warrick RM (2005) Dopamine modulation
818 of two delayed rectifier potassium currents in a small neural network. J
819 Neurophysiol 94:2888-2900.
820 Hajos N, Palhalmi J, Mann EO, Nemeth B, Paulsen O, Freund TF (2004) Spike timing
821 of distinct types of GABAergic interneuron during hippocampal gamma
822 oscillations in vitro. J Neurosci 24:9127-9137.
823 Harris-Warrick RM (2011) Neuromodulation and flexibility in Central Pattern
824 Generator networks. Curr Opin Neurobiol 21:685-692.
825 Harris-Warrick RM, Johnson BR (2010) Checks and balances in neuromodulation.
826 Front Behav Neurosci 4.

827 Harris-Warrick RM, Coniglio LM, Levini RM, Gueron S, Guckenheimer J (1995a)
828 Dopamine modulation of two subthreshold currents produces phase shifts in
829 activity of an identified motoneuron. J Neurophysiol 74:1404-1420.
830 Harris-Warrick RM, Coniglio LM, Barazangi N, Guckenheimer J, Gueron S (1995b)
831 Dopamine modulation of transient potassium current evokes phase shifts in
832 a central pattern generator network. J Neurosci 15:342-358.
833 Hasenstaub A, Shu Y, Haider B, Kraushaar U, Duque A, McCormick DA (2005)
834 Inhibitory postsynaptic potentials carry synchronized frequency
835 information in active cortical networks. Neuron 47:423-435.
836 Hasselmo ME, Bodelon C, Wyble BP (2002) A proposed function for hippocampal
837 theta rhythm: separate phases of encoding and retrieval enhance reversal of
838 prior learning. Neural Comput 14:793-817.
839 Hooper SL (1997a) Phase maintenance in the pyloric pattern of the lobster
840 (Panulirus interruptus) stomatogastric ganglion. J Comput Neurosci 4:191-
841 205.
842 Hooper SL (1997b) The pyloric pattern of the lobster (Panulirus interruptus)
843 stomatogastric ganglion comprises two phase-maintaining subsets. J Comput
844 Neurosci 4:207-219.
845 Hooper SL (1998) Transduction of temporal patterns by single neurons. Nat
846 Neurosci 1:720-726.
847 Hooper SL, Buchman E, Weaver AL, Thuma JB, Hobbs KH (2009) Slow conductances
848 could underlie intrinsic phase-maintaining properties of isolated lobster
849 (Panulirus interruptus) pyloric neurons. J Neurosci 29:1834-1845.
850 Johnson BR, Kloppenburg P, Harris-Warrick RM (2003) Dopamine modulation of
851 calcium currents in pyloric neurons of the lobster stomatogastric ganglion. J
852 Neurophysiol 90:631-643.
853 Johnson BR, Schneider LR, Nadim F, Harris-Warrick RM (2005) Dopamine
854 modulation of phasing of activity in a rhythmic motor network: contribution
855 of synaptic and intrinsic modulatory actions. J Neurophysiol 94:3101-3111.
856 Jordan LM, Slawinska U (2011) Chapter 12--modulation of rhythmic movement:
857 control of coordination. Prog Brain Res 188:181-195.
858 Katz PS (2016) Evolution of central pattern generators and rhythmic behaviours.
859 Philos Trans R Soc Lond B Biol Sci 371:20150057.
860 Kayser C, Montemurro MA, Logothetis NK, Panzeri S (2009) Spike-phase coding
861 boosts and stabilizes information carried by spatial and temporal spike
862 patterns. Neuron 61:597-608.
863 Kiehn O (2016) Decoding the organization of spinal circuits that control locomotion.
864 Nat Rev Neurosci 17:224-238.
865 Kloppenburg P, Levini RM, Harris-Warrick RM (1999) Dopamine modulates two
866 potassium currents and inhibits the intrinsic firing properties of an identified
867 motor neuron in a central pattern generator network. J Neurophysiol 81:29-
868 38.
869 Kopell N, Whittington MA, Kramer MA (2011) Neuronal assembly dynamics in the
870 beta1 frequency range permits short-term memory. Proc Natl Acad Sci U S A
871 108:3779-3784.

872 Krantz SG, Parks HR (2012) The implicit function theorem: history, theory, and
873 applications: Springer Science & Business Media.
874 Kvarta MD, Harris-Warrick RM, Johnson BR (2012) Neuromodulator-evoked
875 synaptic metaplasticity within a central pattern generator network. J
876 Neurophysiol 108:2846-2856.
877 Le Gal JP, Dubuc R, Smarandache-Wellmann C (2017) Coordination of Rhythmic
878 Movements. In: Neurobiology of Motor Control: Fundamental Concepts and
879 New Directions (Hooper SL, Buschges A, eds). Hoboken, New Jersey: Wiley-
880 Blackwell.
881 Lindner B A brief introduction to some simple stochastic processes. Stochastic
882 Methods in Neuroscience 1.
883 Luther JA, Robie AA, Yarotsky J, Reina C, Marder E, Golowasch J (2003) Episodic
884 bouts of activity accompany recovery of rhythmic output by a
885 neuromodulator- and activity-deprived adult neural network. J Neurophysiol
886 90:2720-2730.
887 Ma C, LaMotte RH (2007) Multiple sites for generation of ectopic spontaneous
888 activity in neurons of the chronically compressed dorsal root ganglion. J
889 Neurosci 27:14059-14068.
890 Mamiya A, Nadim F (2004) Dynamic interaction of oscillatory neurons coupled with
891 reciprocally inhibitory synapses acts to stabilize the rhythm period. J
892 Neurosci 24:5140-5150.
893 Mamiya A, Manor Y, Nadim F (2003) Short-term dynamics of a mixed chemical and
894 electrical synapse in a rhythmic network. J Neurosci 23:9557-9564.
895 Manor Y, Nadim F, Abbott LF, Marder E (1997) Temporal dynamics of graded
896 synaptic transmission in the lobster stomatogastric ganglion. J Neurosci
897 17:5610-5621.
898 Manor Y, Bose A, Booth V, Nadim F (2003) Contribution of synaptic depression to
899 phase maintenance in a model rhythmic network. J Neurophysiol 90:3513-
900 3528.
901 Marder E (2012) Neuromodulation of neuronal circuits: back to the future. Neuron
902 76:1-11.
903 Marder E, Bucher D (2001) Central pattern generators and the control of rhythmic
904 movements. Curr Biol 11:R986-996.
905 Marder E, Goaillard JM (2006) Variability, compensation and homeostasis in neuron
906 and network function. Nat Rev Neurosci 7:563-574.
907 Marder E, Bucher D (2007) Understanding circuit dynamics using the
908 stomatogastric nervous system of lobsters and crabs. Annu Rev Physiol
909 69:291-316.
910 Marder E, O'Leary T, Shruti S (2014) Neuromodulation of circuits with variable
911 parameters: single neurons and small circuits reveal principles of state-
912 dependent and robust neuromodulation. Annu Rev Neurosci 37:329-346.
913 Marder E, Bucher D, Schulz DJ, Taylor AL (2005) Invertebrate central pattern
914 generation moves along. Curr Biol 15:R685-699.
915 Markram H, Wang Y, Tsodyks M (1998) Differential signaling via the same axon of
916 neocortical pyramidal neurons. Proc Natl Acad Sci U S A 95:5323-5328.

Masino MA, Fetcho JR (2005) Fictive swimming motor patterns in wild type and mutant larval zebrafish. J Neurophysiol 93:3177-3188.

McLelland D, Paulsen O (2009) Neuronal oscillations and the rate-to-phase transform: mechanism, model and mutual information. J Physiol 587:769-785.

Mouser C, Nadim F, Bose A (2008) Maintaining phase of the crustacean tri-phasic pyloric rhythm. J Math Biol 57:161-181.

Mullins OJ, Hackett JT, Buchanan JT, Friesen WO (2011) Neuronal control of swimming behavior: comparison of vertebrate and invertebrate model systems. Prog Neurobiol 93:244-269.

Nadim F, Manor Y (2000) The role of short-term synaptic dynamics in motor control. Curr Opin Neurobiol 10:683-690.

Nadim F, Bucher D (2014) Neuromodulation of neurons and synapses. Curr Opin Neurobiol 29:48-56.

Nadim F, Booth V, Bose A, Manor Y (2003) Short-term synaptic dynamics promote phase maintenance in multi-phasic rhythms. Neurocomputing 52-4:79-87.

Oren I, Mann EO, Paulsen O, Hajos N (2006) Synaptic currents in anatomically identified CA3 neurons during hippocampal gamma oscillations in vitro. J Neurosci 26:9923-9934.

Panzeri S, Brunel N, Logothetis NK, Kayser C (2010) Sensory neural codes using multiplexed temporal scales. Trends Neurosci 33:111-120.

Peck JH, Gaier E, Stevens E, Repicky S, Harris-Warrick RM (2006) Amine modulation of Ih in a small neural network. J Neurophysiol 96:2931-2940.

Pulver SR, Bayley TG, Taylor AL, Berni J, Bate M, Hedwig B (2015) Imaging fictive locomotor patterns in larval Drosophila. J Neurophysiol 114:2564-2577.

Rabbah P, Nadim F (2007) Distinct synaptic dynamics of heterogeneous pacemaker neurons in an oscillatory network. J Neurophysiol 97:2239-2253.

Rosenbaum P, Marder E (2018) Graded Transmission without Action Potentials Sustains Rhythmic Activity in Some But Not All Modulators That Activate the Same Current. J Neurosci 38:8976-8988.

Schulz DJ, Goaillard JM, Marder E (2006) Variable channel expression in identified single and electrically coupled neurons in different animals. Nat Neurosci 9:356-362.

Skinner FK, Mulloney B (1998) Intersegmental coordination in invertebrates and vertebrates. Curr Opin Neurobiol 8:725-732.

Somogyi P, Klausberger T (2005) Defined types of cortical interneurone structure space and spike timing in the hippocampus. J Physiol 562:9-26.

Soofi W, Goeritz ML, Kispersky TJ, Prinz AA, Marder E, Stein W (2014) Phase maintenance in a rhythmic motor pattern during temperature changes in vivo. J Neurophysiol 111:2603-2613.

Stein PSG (2018) Central pattern generators in the turtle spinal cord: selection among the forms of motor behaviors. J Neurophysiol 119:422-440.

Stein W (2009) Modulation of stomatogastric rhythms. J Comp Physiol A Neuroethol Sens Neural Behav Physiol 195:989-1009.

Tang LS, Taylor AL, Rinberg A, Marder E (2012) Robustness of a rhythmic circuit to short- and long-term temperature changes. J Neurosci 32:10075-10085.

963 Tohidi V, Nadim F (2009) Membrane resonance in bursting pacemaker neurons of
964 an oscillatory network is correlated with network frequency. J Neurosci
965 29:6427-6435.
966 Tseng HA, Nadim F (2010) The membrane potential waveform of bursting
967 pacemaker neurons is a predictor of their preferred frequency and the
968 network cycle frequency. J Neurosci 30:10809-10819.
969 Tseng HA, Martinez D, Nadim F (2014) The frequency preference of neurons and
970 synapses in a recurrent oscillatory network. J Neurosci 34:12933-12945.
971 Vidal-Gadea A, Topper S, Young L, Crisp A, Kressin L, Elbel E, Maples T, Brauner M,
972 Erbguth K, Axelrod A, Gottschalk A, Siegel D, Pierce-Shimomura JT (2011)
973 Caenorhabditis elegans selects distinct crawling and swimming gaits via
974 dopamine and serotonin. Proc Natl Acad Sci U S A 108:17504-17509.
975 Wang XJ (2010) Neurophysiological and computational principles of cortical
976 rhythms in cognition. Physiol Rev 90:1195-1268.
977 Weimann JM, Meyrand P, Marder E (1991) Neurons that form multiple pattern
978 generators: identification and multiple activity patterns of gastric/pyloric
979 neurons in the crab stomatogastric system. J Neurophysiol 65:111-122.
980 Wenning A, Hill AA, Calabrese RL (2004) Heartbeat control in leeches. II. Fictive
981 motor pattern. J Neurophysiol 91:397-409.
982 Wenning A, Norris BJ, Gunay C, Kueh D, Calabrese RL (2018) Output variability
983 across animals and levels in a motor system. eLife 7.
984 Zhang C, Guy RD, Mulloney B, Zhang Q, Lewis TJ (2014) Neural mechanism of
985 optimal limb coordination in crustacean swimming. Proc Natl Acad Sci U S A
986 111:13840-13845.
987 Zhang Y, Bose A, Nadim F (2008) Predicting the activity phase of a follower neuron
988 with A-current in an inhibitory network. Biol Cybern 99:171-184.
989 Zhang Y, Bose A, Nadim F (2009) The influence of the A-current on the dynamics of
990 an oscillator-follower inhibitory network. SIAM J Appl Dyn Syst 8:1564-1590.
991 Zhao S, Sheibanie AF, Oh M, Rabbah P, Nadim F (2011) Peptide neuromodulation of
992 synaptic dynamics in an oscillatory network. J Neurosci 31:13991-14004.

993

Figures

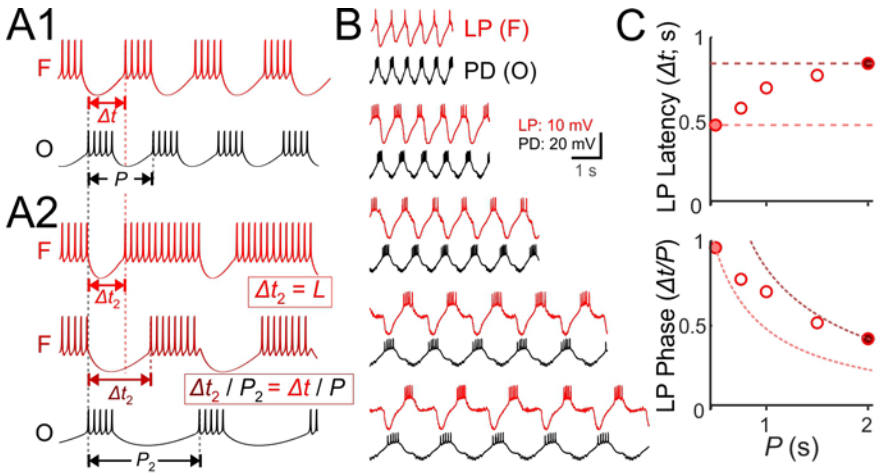

Figure 1: Latency constancy and phase constancy as a function of period

A1. Schematic diagram showing that a follower neuron (F) strongly inhibited by a bursting oscillatory neuron (O) with period *P* can produce rebound bursts with the same period at a latency *Δt*. **A2.** If the period of O changes to a new value (P_2), the new F burst latency (Δt_2) typically falls between two extremes: it could stay constant (top trace) or change proportionally to P_2, so that the burst phase (Δt / *P*) remains constant (middle trace). **B.** Example traces of the pyloric pacemaker PD neuron and the follower LP neuron represent the O and F relationship in panel A. Here, the PD neuron is voltage clamped and a pre-recorded waveform of the same neuron is used to drive this neuron to follow different cycle periods. The LP neuron follows the same period because of the synaptic input it receives. **C.** A measurement of the LP neuron burst onset time (*Δt*) with respect to the onset of the PD neuron burst shows that *Δt* falls between the two limits of constant latency and constant phase. Dotted curves represent constant latency matched to the latencies at the two extreme *P* values.

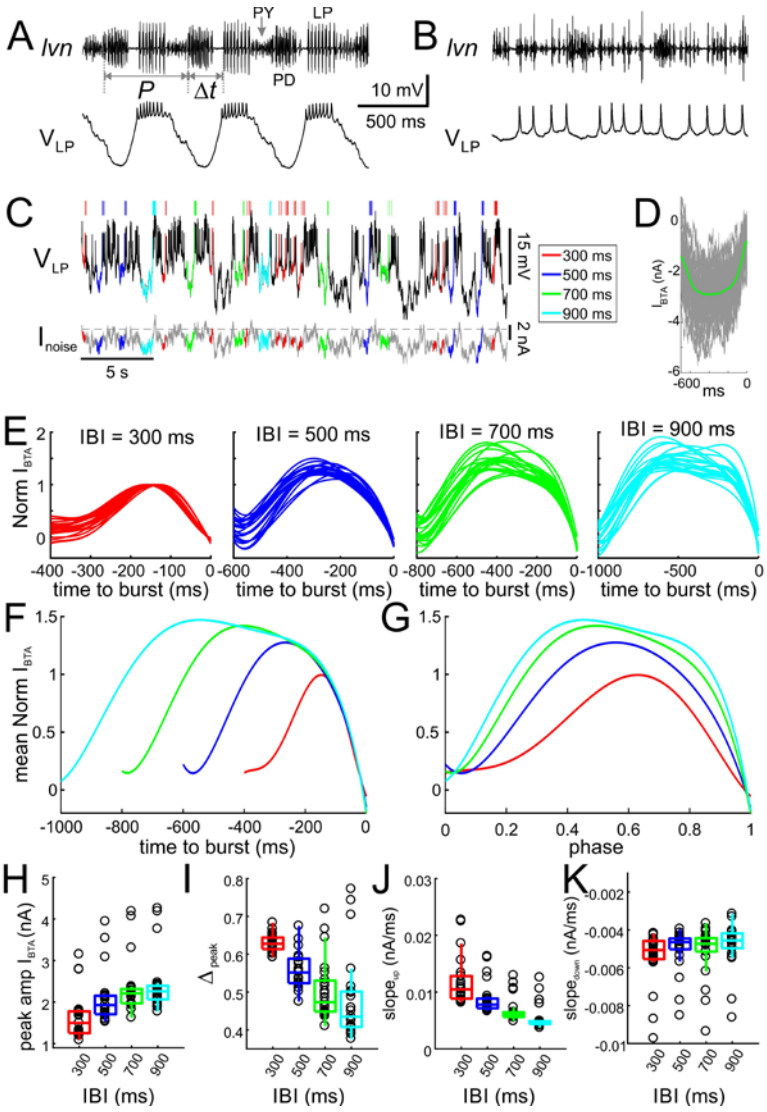

Figure 2: Inputs to the LP neuron influence burst time, spike number and interval
A. Simultaneous intracellular recording of the LP neuron and extracellular recording of the lateral ventricular nerve (*lvn*), containing the axons of the LP, PD and PY neurons (arrows). Period (*P*) and the burst onset time (*Δt*) of the LP neuron are defined in reference to the pacemaker group (PD) burst. **B.** Blocking the AB and PY synaptic inputs (10 μM picrotoxin) to the LP neuron disrupts its bursting oscillations. **C.** The LP neuron, in picrotoxin, was driven with a noise current input (I_{noise}) for 60 minutes. In response, the LP neuron produced an irregular pattern of bursting. Specific inter-burst intervals (*IBI*s) were tagged and used for burst-triggered averaging. **D.** Example of burst-trigger-averaged input current (I_{BTA}, green). Individual traces are shown in grey. **E.** For each *IBI* (300, 500, 700, 900 ms), I_{BTA} was calculated and normalized to the (negative) peak value of I_{BTA} for *IBI*=300 ms. Different traces in each panel show the I_{BTA} of different preparations. **F.** The mean (across preparations) of the normalized I_{BTA}s shown in panel E. **G.** Traces in panel F normalized by *IBI*. **H-K.** Four parameters define the shape of the I_{BTA}: peak amplitude I_{amp} (**H**), peak phase Δ_{peak} (**I**), $slope_{up}$ (**J**) and $slope_{down}$ (**K**) across preparations. IBI had a significant effect on amplitude I_{amp} ($p<0.001$), peak phase Δ_{peak} ($p<0.001$), $slope_{up}$ ($p<0.001$) and $slope_{down}$ ($p=0.002$).

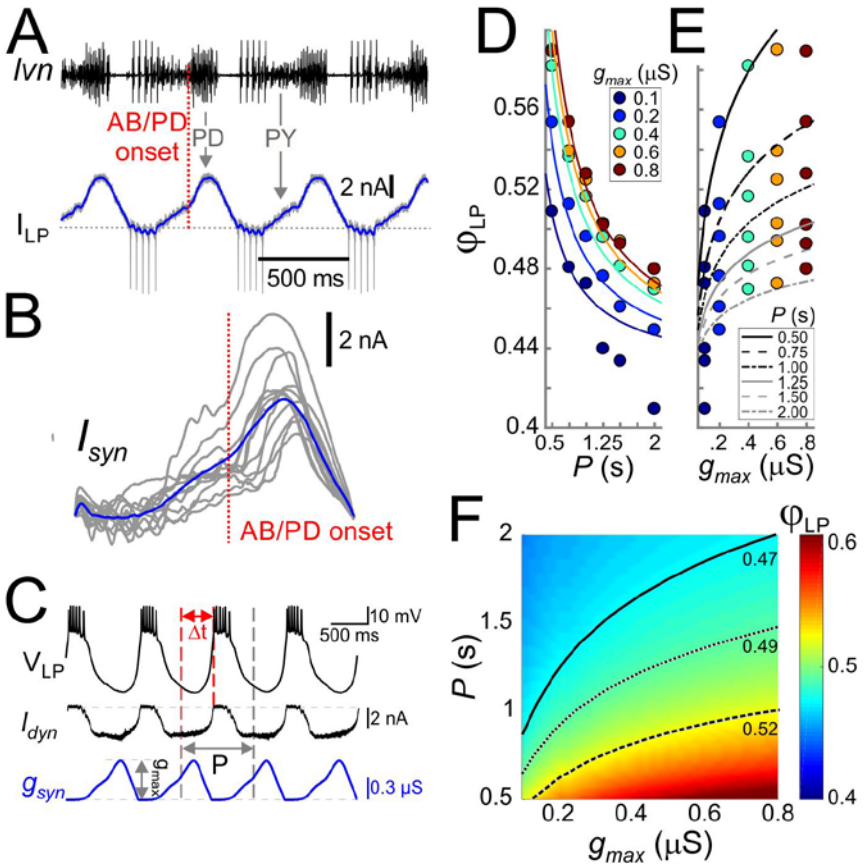

Figure 3: Cycle period and synaptic strength affect the phase of LP burst onset in opposite directions.

A. The synaptic input to the LP neuron was measured by voltage clamping it at a holding potential of -50mV during ongoing oscillations. The onset of the pacemaker (AB/PD) activity is seen as a kink in the synaptic current (I_{LP}, blue). Dashed line: 0 nA. **B.** Synaptic input averaged across (last 5 of 30) cycles from 9 different LP neurons. Traces are aligned to the onset of the PD neuron burst (dotted vertical red line; see panel A), normalized by the cycle period and terminated at the end of the downslope (coincident with the first LP action potential when present). The blue trace shows the average. **C.** An example of the LP neuron driven by the realistic synaptic waveform in dynamic clamp. The burst onset time (Δt) was measured relative to the AB/PD onset and used to measure the LP phase (φ_{LP}). g_{max} denotes the conductance amplitude. **D.** Mean φ_{LP} (N=9 preparations) shown as a function of P and fit with the function given by Equation (8) (fit values τ_s = 26.0 ms, g^* = 0.021 µS and $\Delta_{peak} \cdot DC$ = 0.43). **E.** Mean φ_{LP} plotted against g_{max} also shown with the fit to Equation (8). **F.** Heat map, obtained from fitting Equation (8) to the data in panels D and E, shows φ_{LP} as a function of both g_{max} and P. Black curves show the level sets of phase constancy for three values of φ_{LP} (0.47, 0.49, and 0.52).

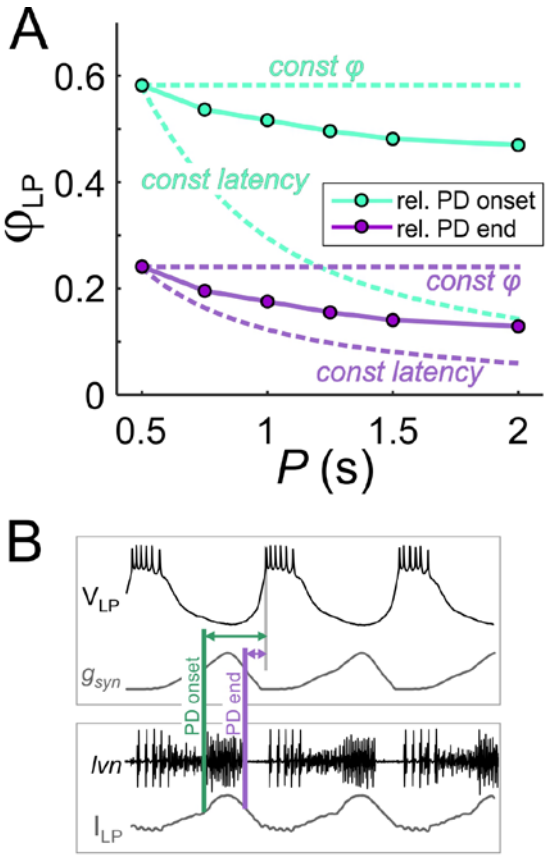

Figure 4: The constant duty cycle of synaptic conductance is a major factor in phase maintenance.

A. The change in φ_{LP} values with P are compared with the constant phase (solid curve) and constant latency (dashed curve) extremes. Lime traces show the usual values of φ_{LP}, calculated from the LP burst onset latency with respect to the onset of the PD burst. Lavender traces show φ_{LP} calculated from the LP burst onset latency with respect to the end of the PD burst. Data shown are the same as in Fig. 3D for g_{max}=0.4 µS. **B.** Schematic diagram shows the latency of LP burst onset measured with respect to the (estimated) onset and end of the PD burst in the dynamic clamp experiments (see Methods). Bottom panel shows the synaptic current waveform measured in the voltage-clamped LP neuron during ongoing pyloric activity. Top panel shows the dynamic clamp injection of the synaptic conductance waveform into the LP neuron. The current waveform of the bottom panel is aligned to the conductance waveform of the top panel for the comparison used in determining the PD burst onset and end in the top panel.

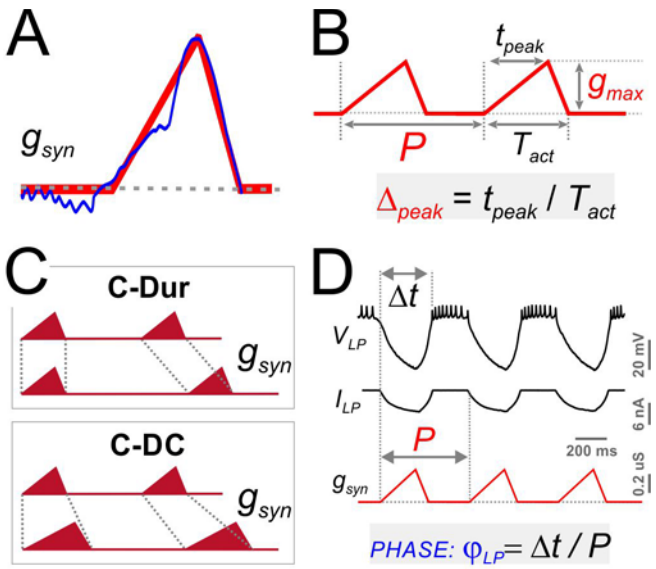

Figure 5: Four parameters describing synaptic shape were varied in the experimental paradigm.
A. A triangle shaped conductance was used to mimic the synaptic input to the LP neuron. **B.** The triangular waveform can be described by period (P), duration (T_{act}), peak time (t_{peak}) and amplitude (g_{max}). **C.** In dynamic clamp runs, the synapse duration T_{act} was kept constant at 300 ms (C-Dur) or maintained at a constant duty cycle (T_{act} /P) of 0.3 (C-DC) across all values of P. **D.** Intracellular voltage recording of the LP neuron during a dynamic clamp stimulation run using the triangle conductance (in picrotoxin). The burst onset time (Δt, calculated in reference to the synaptic conductance onset) was used to calculate the activity phase ($\varphi_{LP} = \Delta t/P$).

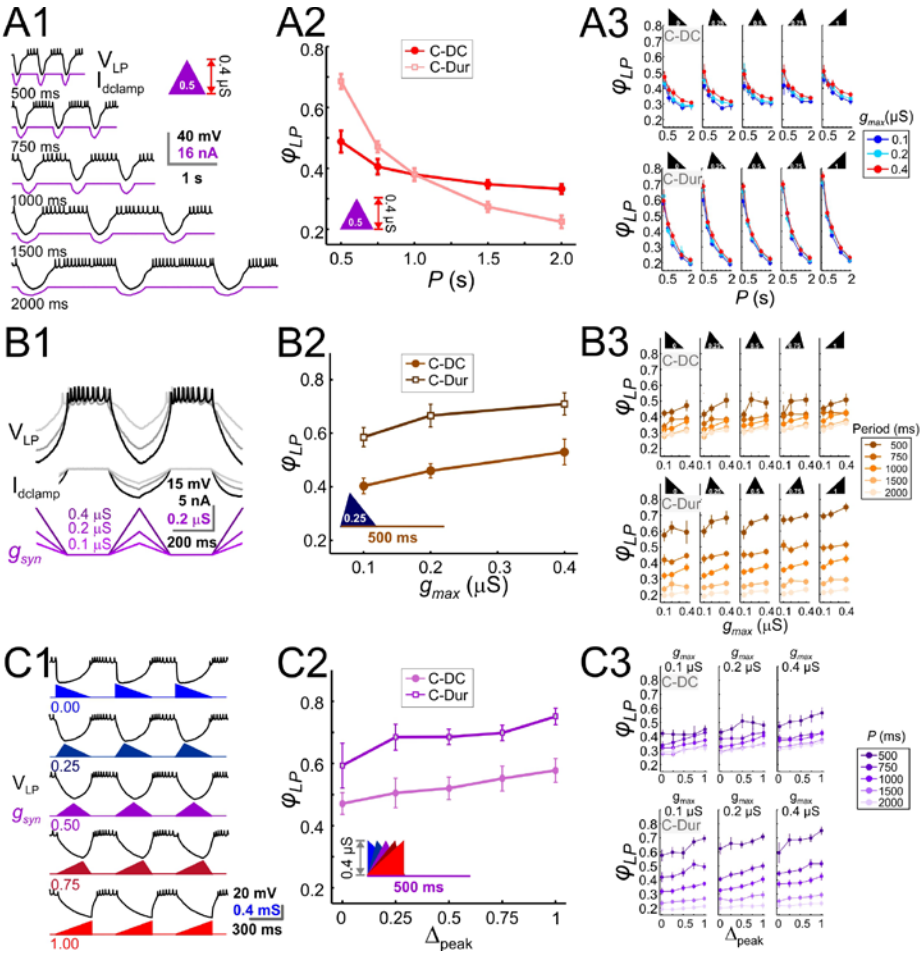

Figure 6: The LP burst onset phase decreases as a function of P, but increases as a function of g_{max} and Δ_{peak}.
Periodic injection of an inhibitory triangular waveform conductance into the LP neuron (in picrotoxin) produced bursting activity from which φ_{LP} was calculated. The parameters g_{max}, Δ_{peak} and P were varied across runs for both C-Dur and C-DC cases. **A.** φ_{LP} decreases as a function of P. **A1.** Intracellular recording of an LP neuron showing a C-DC conductance input across five periods. **A2.** φ_{LP} for the example shown in A1 plotted as a function of P (for g_{max} = 0.4 µS, Δ_{peak} = 0.5) for both C-Dur and C-DC cases. φ_{LP} decreases rapidly with P and the drop is larger for the C-Dur case. **A3.** φ_{LP} decreased with P in both the C-DC case (Three-Way RM ANOVA, p<0.001, F=100.7) and the C-Dur case (Three-Way RM ANOVA, p<0.001, F=466.4) for all values of Δ_{peak}. The range of φ_{LP} drop was greater for the C-Dur case compared to the C-DC case. **B.** φ_{LP} increases as a function of g_{max}. **B1.** Intracellular recording of an LP neuron showing the conductance input across three values of g_{max}. **B2.** φ_{LP} for the example shown in B1 plotted as a function of P (for P = 500 ms, Δ_{peak} = 0.25) shows a small increase for both C-Dur and C-DC cases. **B3.** φ_{LP} increased with g_{max} in almost all trials for both C-DC and C-Dur cases and all values of Δ_{peak}. **C.** φ_{LP} increases as a function of Δ_{peak}. **C1.** Intracellular recording of the LP neuron showing the conductance input for five values of Δ_{peak}. **C2.** φ_{LP} for the example neuron in C1 plotted as a function of Δ_{peak} (for P = 500 ms, g_{max} = 0.4 µS) for both C-DC and C-Dur cases. **C3.** φ_{LP} increased with Δ_{peak} for both C-DC and C-Dur cases and for all values of g_{max}. In all panels, error bars show standard deviation.

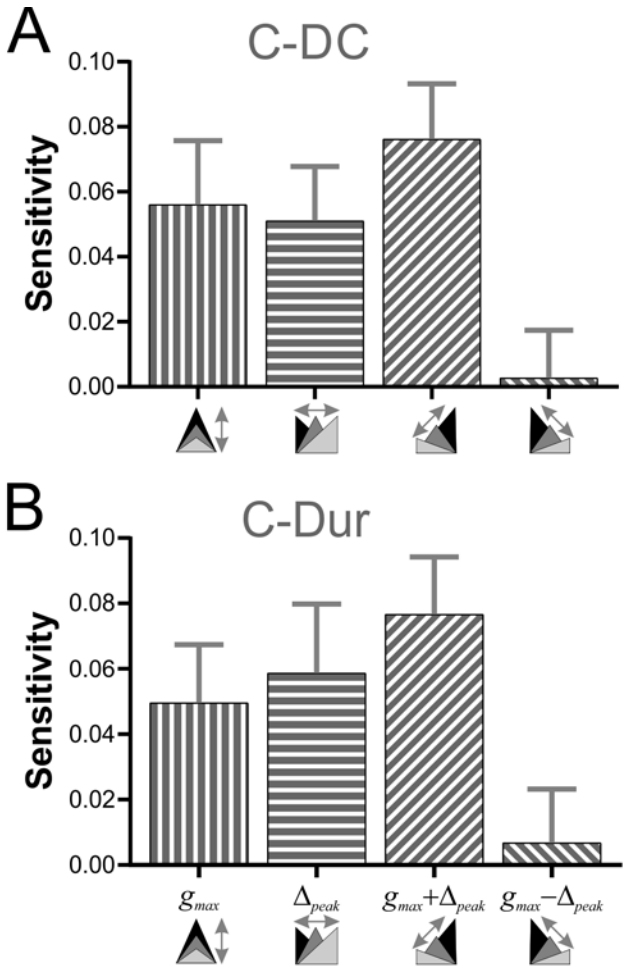

Figure 7: Sensitivity analysis shows that φ_{LP} increases more effectively if g_{max} and Δ_{peak} increase together.
A. The sensitivity of φ_{LP} to local changes in g_{max} and Δ_{peak} was averaged across all values of P for the C-DC case. Sensitivity was largest if both parameters were increased together ($g_{max} + \Delta_{peak}$) and smallest if they were varied in opposite directions ($g_{max} - \Delta_{peak}$; One-Way RM-ANOVA, $p<0.001$, $F=3.330$). **B**. The same sensitivity analysis in the C-Dur case shows similar results (One-Way RM-ANOVA, $p<0.001$, $F=2.892$). In both panels, error bars show standard deviation.

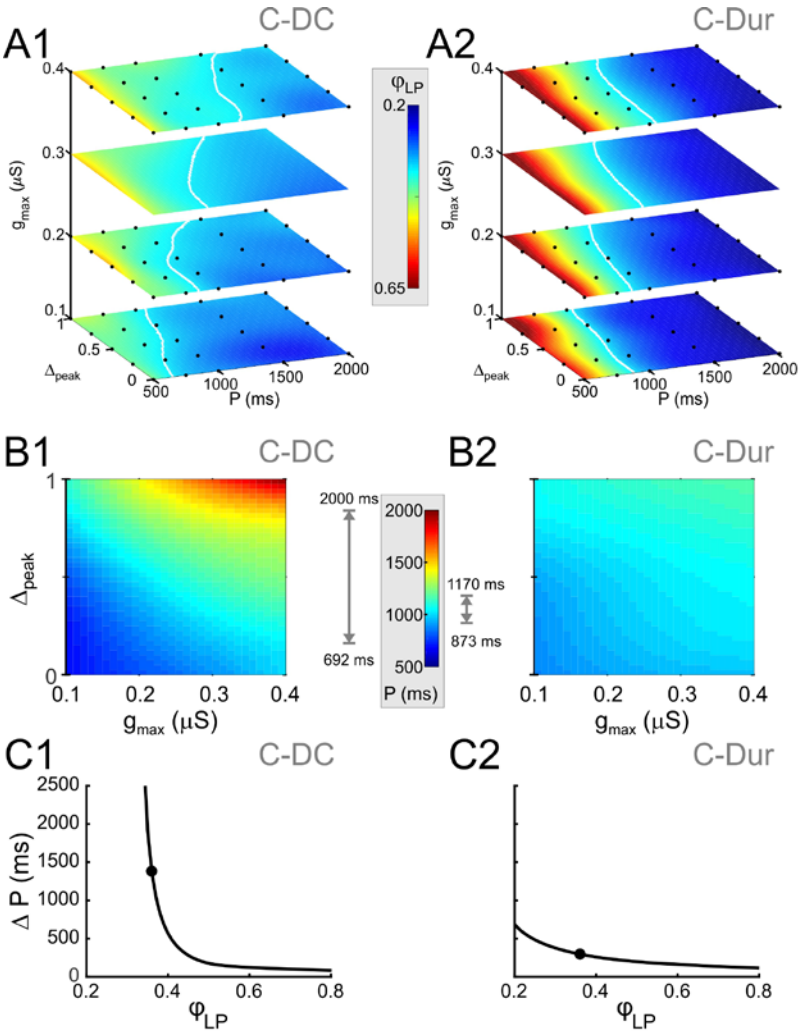

Figure 8: Simultaneous increase of both Δ_{peak} and g_{max} across their range of values can produce phase maintenance across a large P range in the C-DC case and a much smaller P range in the C-Dur case

A. Heat map plots of the function Φ (see Methods), plotted for the range of values of *P* and Δ_{peak} and 4 values of g_{max} for the C-DC (**A1**) and C-Dur (**A2**) cases. The white curves show the level set of φ_{LP} = 0.34, shown as an example of phase constancy. The color maps are interpolated from sampled data (see Methods; N=9 experiments). The locations of the sampled data are marked by black dots. **B.** Heat map for the level sets φ_{LP} = 0.34 for the C-DC (**B1**) and C-Dur (**B2**) cases. Range of colors in each panel indicate the range of *P* values for which φ_{LP} could remain constant at 0.34 for each case, as indicated by the grey arrows on the side of the heatmap color legend. **C.** The range (ΔP) of *P* values for which φ_{LP} could remain constant at any value between 0.2 and 0.8 for the C-DC (**C1**) and C-Dur cases (**C2**). Filled circles show the values shown in panel B. The LP neuron cannot achieve φ_{LP} values below 0.3 in the C-DC case. For φ_{LP} values between 0.3 and ~0.65, the range was larger in C-DC case.

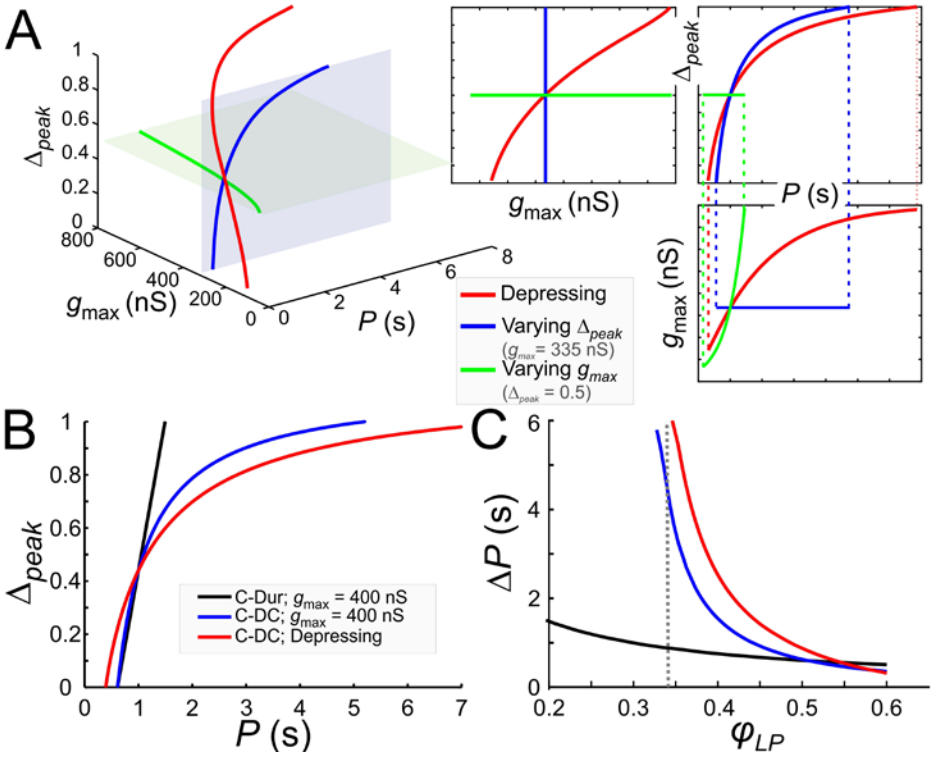

Figure 9: Model prediction of the range of phase constancy.
A. For the C-DC case, a constant phase of φ_{LP} = 0.34 can be maintained across a range of cycle periods P when g_{max} is constant (at 335 nS; blue plane) and Δ_{peak} varies from 0 to 1 according to Equation (11) (blue), or when Δ_{peak} is fixed (at 0.5; green plane) and g_{max} varies from 200 to 800 nS according to Equation (10). Alternatively, g_{max} and Δ_{peak} can covary to maintain phase, as in a depressing synapse, where g_{max} varies with P according to Equation (16), and Δ_{peak} is calculated for each P and g_{max} value according to Equation (11). As seen in the 2D coordinate-plane projections of the 3D graph (right three graphs), the range of P values for which phase constancy is achieved is largest when g_{max} and Δ_{peak} covary (dotted lines show limits of P for phase constancy). The depressing synapse conductance is chosen to be 335 nS at P = 1 s. **B, C.** A comparison between the C-DC and C-Dur cases shows that in the latter case a constant phase of φ_{LP} can be maintained across a larger range of P values when Δ_{peak} increases with P (and g_{max} is fixed at 400 nS) according to Equation (11). The relationship of Δ_{peak} and P is shown in **B** for φ_{LP} = 0.34. **C** shows the range of P values (ΔP) of cycle periods for which phase remains constant at φ_{LP}. If g_{max} also varies with P, as in a depressing synapse (red; Equation (16)), the range of P values for which phase is constant is further increased. (Dotted line: φ_{LP} = 0.34.)

Source Data Files

Figure 2-1. *File: Figure2_sourcedata.xlsx*
This Excel file contains 4 sheets, including all measured attributes of the burst-triggered average current (I_{BTA}) for different IBIs (N=23) as shown in Fig. 2H-2K.

Figure 7-1. *File: Figure7_sourcedata.xlsx*
This Excel file contains 2 sheets for the C-DC and C-Dur cases. These sheets include all sensitivity values for each value of P, at each g_{max} and each Δ_{peak} in all 8 directions: ($+g_{max}$, $+\Delta_{peak}$, $-g_{max}$, $-\Delta_{peak}$, $+g_{max}$ & $+\Delta_{peak}$, $-g_{max}$ & $-\Delta_{peak}$, $+g_{max}$ & $-\Delta_{peak}$, $+g_{max}$ & $-\Delta_{peak}$). Fig. 7 shows the sensitivities, averaged across all P values, and averaged across aligned directions: [$+g_{max}$ and $-g_{max}$]; [$+\Delta_{peak}$ and $-\Delta_{peak}$]; [$+g_{max}$ & $+\Delta_{peak}$ and $-g_{max}$ & $-\Delta_{peak}$]; [$+g_{max}$ & $-\Delta_{peak}$ and $+g_{max}$ & $-\Delta_{peak}$].